

NIST-GCR-95-679

**A REVIEW OF FLOWS DRIVEN BY
NATURAL CONVECTION IN ADIABATIC
SHAFTS**

Edward E. Zukoski

Department of Mechanical Engineering
California Institute of Technology
Pasadena, CA 91125
October 1995



U.S. Department of Commerce
Ronald H. Brown, *Secretary*
Technology Administration
Mary L. Good, *Under Secretary for Technology*
National Institute of Standards and Technology
Arati Prabhakar, *Director*

Notice

This report was prepared for the Building and Fire Research Laboratory of the National Institute of Standards and Technology under grant number 60NANB6D1444. The statement and conclusions contained in this report are those of the authors and do not necessarily reflect the views of the National Institute of Standards and Technology or the Building and Fire Research Laboratory.

A Review of Flows Driven by Natural Convection in Adiabatic Shafts.

**Edward E. Zukoski
Professor of Mechanical Engineering
California Institute of Technology
Pasadena, California 91125**

10/07/94

**This review has been carried out with the support of a grant from the
U.S. Department of Commerce
National Institute of Science and Technology
Building and Fire Research Laboratory**

A Review of Flows Driven by Natural Convection in Adiabatic Shafts.

1. Introduction	Page 3
2. Stack effect	5
3. Turbulent mixing Process	11
4. Experimental Apparatus	17
5. Modeling	18
6. Experimental Results	32
7. Conclusions	43

1. INTRODUCTION

An experimental study of the motion of hot gas through vertical shafts and passages under the influence of buoyancy forces is being made with the support of the Building and Fire Research Laboratory of the National Institute of Science and Technology, the Department of Commerce. The aim of this work is to derive the information required for the preparation of models which can be used to describe these flows in computer-based models of fire spread through structures.

As a part of this work, this review has been made of the experimental and analytic study carried out from 1973 to 1976 by Drs. Jonnie B. Cannon and Edward. E. Zukoski under a grant from the program entitled Research Applied to National Needs sponsored by the National Science Foundation . The aim of this work, reported in detail in Cannon and Zukoski (1976)¹, see foot note, was to study the vertical penetration of hot buoyant gas into a shaft initially filled with colder and more dense air. The movement of light gas is produced by a turbulent mixing mechanism that is related to the Rayleigh Taylor mixing process.

The origin of Cannon's and Zukoski's interest in the flow discussed is the motion of buoyant masses of hot gas produced during accidental fires that are confined within vertical shafts. Buoyant flows of this type occur in spaces such as shafts, stairwells, and atria, in which the height-to-width ratio of the space is large. In many of these situations, the location of openings between the shaft and the outside world and the nature of the source of the buoyant fluid can have a critical effect on the flow. The flows are important since they transport toxic gases vertically throughout a building and the transport process is independent of the stack effect and hence does not depend on the presence of openings connecting the interior and exterior of the building.

Two mechanisms are primarily responsible for vertical motion of buoyant gas within a building: The first occurs in shafts that are open at various levels to the surrounding atmosphere. The gas motion is produced by pressure

¹ Cannon, Jonnie. B. and Zukoski, Edward. E., (1975), *Turbulent Mixing in Vertical Shafts Under Conditions Applicable to Fires in High Rise Buildings*, Technical Fire Report No. 1 to the National Science Foundation, California Institute of Technology, Pasadena, California.

differences that result from density differences between the gas on the inside of the shaft and the ambient atmosphere on the outside. This mechanism is often called the *stack effect*.

This mechanism is well understood and has been the subject of many studies and is used extensively in solving flow problems involving heating and ventilation systems as well as in making computations regarding the motion of smoke. The first section of this review is a very brief overview of the motion produced by the simple adiabatic stack effect. This section is included so that its effect and that produced by the buoyancy driven mixing can be contrasted and compared.

The second mechanism arises because the interface between an upper layer of cold and therefore more dense gas, and a lower layer of hot and therefore less dense gas, is unstable to small disturbances in the interface position. The instability leads to a rapid mixing between the two gas layers, and this mechanism operates in the absence and presence of leaks in the shaft.

This second process is identified here as the *turbulent mixing process* and it is related to the Rayleigh-Taylor mixing process² that has been studied extensively. However, this earlier work has usually involved systems in which the vertical dimension was much smaller than the horizontal where as, for the flows of interest here in the fire context, the vertical dimension is much larger than the horizontal. We are also interested in the transient development of the mixing process and the emphasis in earlier work has been on steady processes.

The second mechanism is the focus of the present review. The much better understood and better known stack effect is discussed below in Section 1 so that its effect can be contrasted with the second mechanism discussed here. Up to this time, the turbulent mixing process has not been studied to the depth required to suggest simple models that include heat transfer between the gas involved in the flows and the surrounding walls.

² Koschmieder (1993), *Benard Cells and Taylor Vortices*, Cambridge U. Press

2. ADIABATIC STACK EFFECT

Flows of buoyant gas within buildings depend in detail on the location of leaks in walls, floors and ceilings that connect internal compartments, the effects produced by forced ventilation systems, and the external pressure field that results from wind. Several greatly simplified examples are discussed here to illustrate the flows of interest to us.

Shaft with openings at bottom and top: The flow in a well sealed shaft resembles that in a chimney when the turbulent mixing process of primary interest to us is ignored. A simplified configuration, shown in the sketch of Figure 1, is analyzed in the following paragraphs. Here, the shaft is sealed except at the bottom and at an window near the top at elevation H . The bottom of the shaft is open to a very large area filled with hot gas that is exposed to the ambient atmosphere.

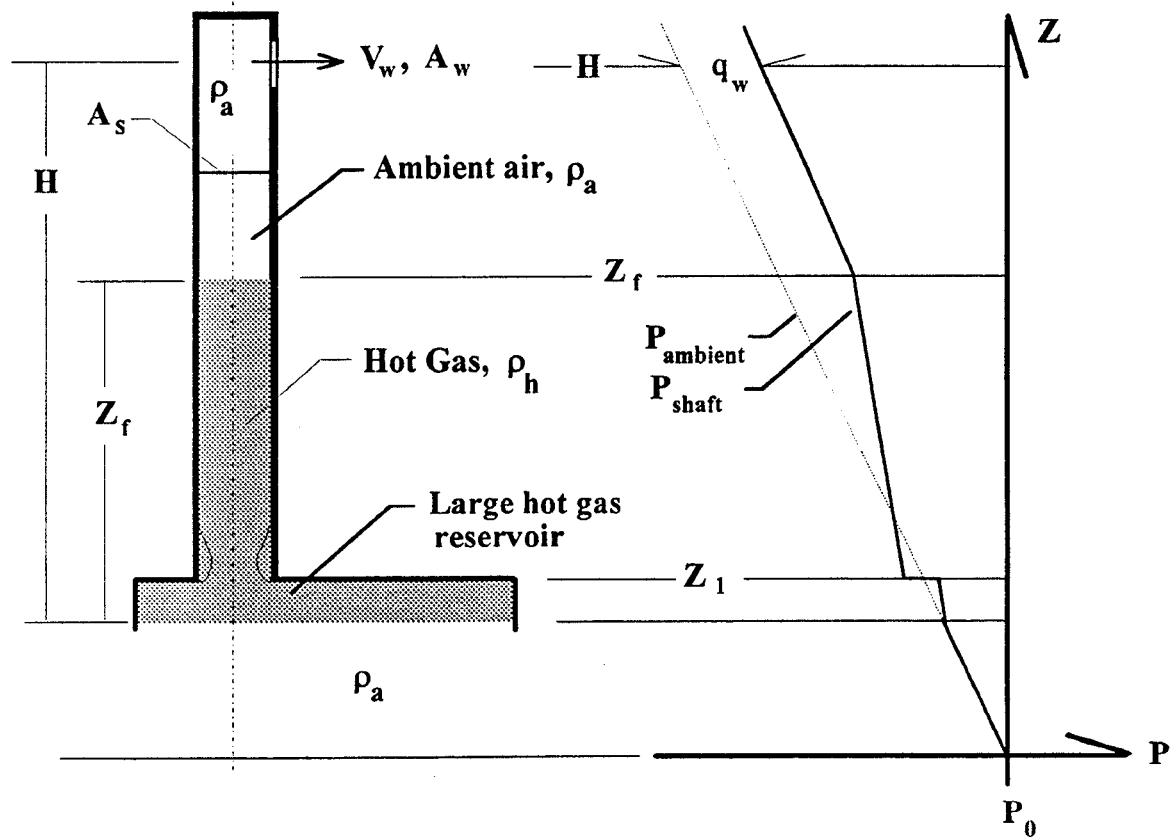


Figure 1. Adiabatic Stack Effect.

The sketch shows the flow some time after the hot gas has entered the shaft. The pressure distribution within the shaft, $P_s = P_{\text{shaft}}$, and that outside the shaft, $P_{\text{ambient}} = (\text{the ambient pressure}) = P_a$, are shown at the right. Heat transfer effects are ignored here completely. In the absence of strong dynamic effects, the pressure distributions in the shaft and ambient

atmosphere are fixed by the gravitational term, $\left(\frac{dP}{dZ}\right) = -\rho g$, and thus the pressure falls more slowly in the regions in which the density is smaller.

We assume that the reservoir of hot gas at the bottom is so large that, as gas flows from it into the shaft, the upward motion of the interface with the ambient air is negligible. We also ignore heat transfer effects between gas and wall that would change the density of the hot gas. The first of these approximations can easily be taken into account as accurately as required and without greatly complicating the results; the second can not easily be accommodated because the inclusion of the heat transfer processes complicates the computation.

The sharp pressure drop at elevation Z_1 is produced by the flow of hot gas from the large reservoir and into the shaft. The drop is assumed to be equal to the dynamic pressure q_s of the flow in the shaft with velocity V_s , $(1/2 \rho_a V_s^2)$, and any complexity resulting from flow separation at the bottom of the shaft in the entrance region is ignored here. In the following calculations, we assume that dynamic pressure is not recovered. The shaft and window have cross section areas of A_s and A_w and for simplicity in notation, A_w includes the *vena contracta* area reduction at the window exit. The flow is assumed to be one-dimensional; ρ_a and ρ_h are the density of the ambient gas and that of the hot gas in the shaft; Z_f is the elevation of the front of the hot gas flow; and $P_s\{Z_f\}$ and $P_a\{Z_f\}$ are the pressures inside and outside of the shaft at elevations Z_f .

A simple pressure balance gives the result,

$$P_s\{Z_f\} - P_a\{Z_f\} = q_w = (\rho_a - \rho_h)gZ_f - q_s \quad (1)$$

$$\text{when } q_w \equiv \frac{1}{2}\rho_a V_w^2 \quad \text{and} \quad q_s \equiv \frac{1}{2}\rho_h V_s^2$$

For the configuration shown here, continuity arguments give:

$$\rho_w A_s V_s \equiv \rho_w A_s \left(\frac{dZ_f}{dt} \right) = \rho_w A_w V_w \quad (2)$$

We have assumed here that the front of the hot gas acts like a piston that drives the unheated gas in front of it with the speed of the front and without mixing. Since we ignore the effect of the pressure on the density of the gas, the velocities of the hot and cold gas within the shaft are equal. Using the definition that

$$(\Delta\rho_i/\rho_w) \equiv (\rho_a - \rho_h)/\rho_a = (1 - [\rho_h/\rho_a]) \approx (1 - [T_a/T_h]),$$

these equations can be combined to give the results that

$$\left(\frac{dZ_f}{dt} \right) = \left(\frac{A_w}{A_s} \right) \sqrt{2 \left(\frac{\Delta\rho_i}{\rho_w} \right) g} (Z_f)^{\frac{1}{2}} \left(\frac{1}{1 + \frac{1}{2} \left(\frac{\rho_h}{\rho_w} \right) \left(\frac{A_w}{A_s} \right)^2} \right)$$

and integration gives:

$$Z_f = \left(\sqrt{Z_1} + \left[\left(\frac{A_w}{A_s} \right) \sqrt{\frac{1}{2} \left(\frac{\Delta\rho_i}{\rho_w} \right) g} \right] (t) \left(\frac{1}{\sqrt{1 + \frac{1}{2} \left(\frac{\rho_h}{\rho_w} \right) \left(\frac{A_w}{A_s} \right)^2}} \right) \right)^2$$

When Z_1 and A_w/A_s are small enough, this equation can be rewritten in terms of the time required for the front to rise from the bottom of the shaft to reach height of the window at Z_f as:

$$t\{Z_f\} = \left(\frac{A_s}{A_w}\right) \sqrt{\frac{2H}{\left(\frac{\Delta\rho_i}{\rho_w}\right)g}} \sqrt{\frac{Z_f}{H}} \quad (3)$$

The height of the shaft, H , drops out of this result.

The time required for the front to reach a given elevation is proportional to the area ratio and the square root of the elevation above the starting position of the front. Thus, if the leakage area A_w is reduced by a factor of 10, the time required will be increased by this factor.

The results in Equations 3 and 4 are useful for comparison with the times required for the mixing layer to propagate up shafts. However, remember that heat transfer results are not included here.

Example 1: Consider a shaft with an open window at $H = 30 \text{ m} = Z_{f\{final\}}$, with $A_s = 10 \text{ m}^2$ and $A_w = 1 \text{ m}^2$, i.e., with $A_s/A_w = 10$, and with $\rho_a/\rho_h = 1.33$ or $\Delta\rho/\rho_a = 0.25$. We find from Equation 4 that the time required by the front to reach 30 m level will be about 50 s.

If the area of the leak were reduced to 1% of the shaft cross section area, the time would increase to 500 s.

Distributed Leaks from Shaft: Most structures have leaks that average a few percent of the surface area of the shaft per floor. A simple calculation, similar to that described above, based on the assumption that the shaft wall has an opening with a constant width δ that extends from the bottom at $Z = 0$ to the top of the shaft at $Z = H$, leads to the result that, for a given total open area, $A_w = H\delta$, the time required for the front to reach a given height will

be as given by:

$$t\{Z_f\} = \left(\frac{A_s}{\delta H} \right) \left(\sqrt{\frac{H}{2 \left(\frac{\Delta \rho_i}{\rho_w} \right) g}} \right) \ln \left(\frac{1 + \sqrt{Z_f/H}}{1 - \sqrt{Z_f/H}} \right) \quad (4)$$

which reduces to the previous result when $(Z_f/H) \ll 1.0$. However, H does not drop out of this equation.

Example 2: If the shaft described in the previous case has a perimeter of 12 m and is 30 m high, and if 1% of the surface area is open, the total open area, $H\delta$ would be 3.6 m² distributed over the height of the shaft. If $Z_f/H = 0.8$, or 0.9 then $t\{Z_f\}$ will be about 40 or 50 s. These values are comparable with those found in Example 1, for which the single window had a much smaller area. If the window in Example 1 had been 3.6 m, the time required for the smoke to reach that level would have been about 14 s.

This difference is caused by the reduction in open area available for the exit of air from the shaft, that occurs in the second example, as the hot gas rises in the shaft.

Affects of Wind: The effects of winds on the flow of gas within the building can be dominant and they are illustrated by returning to the problem of Example 1. Here the pressure difference between the inside and outside of the building at the window level ΔP_S was approximately $(\Delta \rho_i g H)$ and the dynamic pressure q_w of the wind with a velocity W will be $[(1/2)(\rho_a W^2)]$. If the wind speed is 10 m/s and the other parameters are as given in Example 1, the ratio of the pressure difference produced by the stack effect to the dynamic pressure of the wind, $(\Delta P_S / q_w)$ will be about 1.5. Since the pressure difference across a building due to wind can be from 1 to 1.5 q_w , it is clear that the wind effects can be comparable to the stack effect. Thus, in general, wind conditions can have an important effect on flows throughout the building and, in particular, in shafts that are ventilated by leaks into the building or to the outside.

Computation of the pressure field imposed by wind effects on the exterior surfaces of buildings is a complicated process and depends in detail on the geometry of the building, the direction and magnitude of the wind velocity, and the influence of adjoining structures and topography on the flow field.

A very large body of data, computer programs, and reports has been developed concerning the stack effect, with and without wind effects, and the influences of building design on motion of gas within a building. See, for example, the on going work by John H. Klote at NIST and also:

Klote, J. H., *A Computer Program for Analysis of Pressurized Stairwells and Pressurized Elevator Shafts*, National Bureau of Standards (U.S.), NBSIR 80-2157.

Klote, J. H. and Bodart, X., *Smoke Control by Pressurized Stairwell - Computer Analysis Put to the Test*, Journal of CIB, Vol 12, No. 4, July/August 1984.

Klote, J. H. and Fothergill, J. W., *Design of Smoke Control Systems for Buildings*, National Bureau of Standards (U.S.), NBS-Handbook 141, June 1983.

Kusuda, T. and Ochifugi, K., *Air Leakage and Smoke Migration Calculations for NBS Administration Building*, Bldg. Thermal System Div., Center of Building Tech., Nat. Eng. Lab., NBS, October 1979.

Lawson, D. I. (editor) *Symposium No. 4, Movement of smoke on escape routes in buildings*, Proceedings of the Symposium held at Watford College of Technology, U.K., on 9th and 10th April, 1969.

Veers, E. and Waterhouse, A. *A computer model for analyzing smoke movement in buildings*, Building Research Establishment Current Paper, Fire Research Station, Borehamwood, Hertsfordshire, WD6 2BL, England, November 1978.

3. The TURBULENT MIXING PROCESS

Important features of the turbulent mixing process that can occur in an accidental fire within a shaft are identified in the scenario shown in Figure 2 in which a fire is started at the bottom of a vertical shaft. Pressures, both on the centerline of the shaft and outside of the shaft, and density maps that apply to the conditions shown in Figure 2(c) are shown in Figure 3. The assumptions made here that the pressure at the bottom of the shaft is the ambient value, that dynamic effects are negligible, and that the densities in the upper layer, ρ_U , and ceiling layer, ρ_C , are less than that in the ambient atmosphere, ρ_a .

At first, the shaft is only open to the outside air through a large door at the bottom floor level and the window at the top right-hand side of the shaft remains closed until sketch of Figure 2(d). Thus, leaks are ignored and the stack effect is absent until the window is opened.

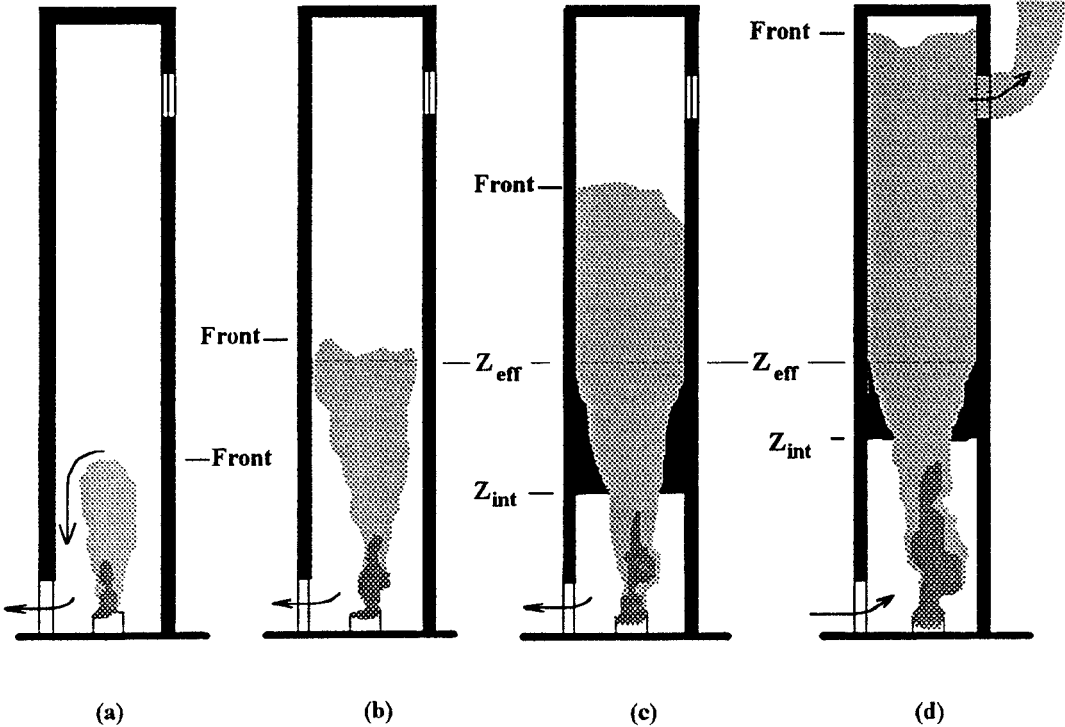


Figure 2. Fire Plume in a Shaft, Open at Bottom.

In 2(a), a small fire has been ignited and a plume has started to rise into the cooler air in the shaft. This plume can entrain unheated air all along its

border and behaves like a freely rising buoyant plume until the edges of the plume approach the walls of the shaft. During this phase of the flow, the plume grows in volume due to heat addition from the fire and entrainment of cool air from the room. The unsteady growth of the plume can be modeled satisfactorily as long as wall effects are ignored, but interactions between the plume and the wall can not be handled satisfactorily now.

The growing plume in Figure 2(a) entrains some of the gas originally in the room and also displaces unheated air in the shaft and forces it to leave the shaft through the door. The heat added to the gas within the shaft must be equal to the enthalpy carried out of the room by the gas that leaves through the doorway. Much of this displaced air comes from above the head of the plume and the total mass that must leave the shaft to maintain atmospheric pressure within the shaft is proportional to the net heat transfer to the gas within the shaft.

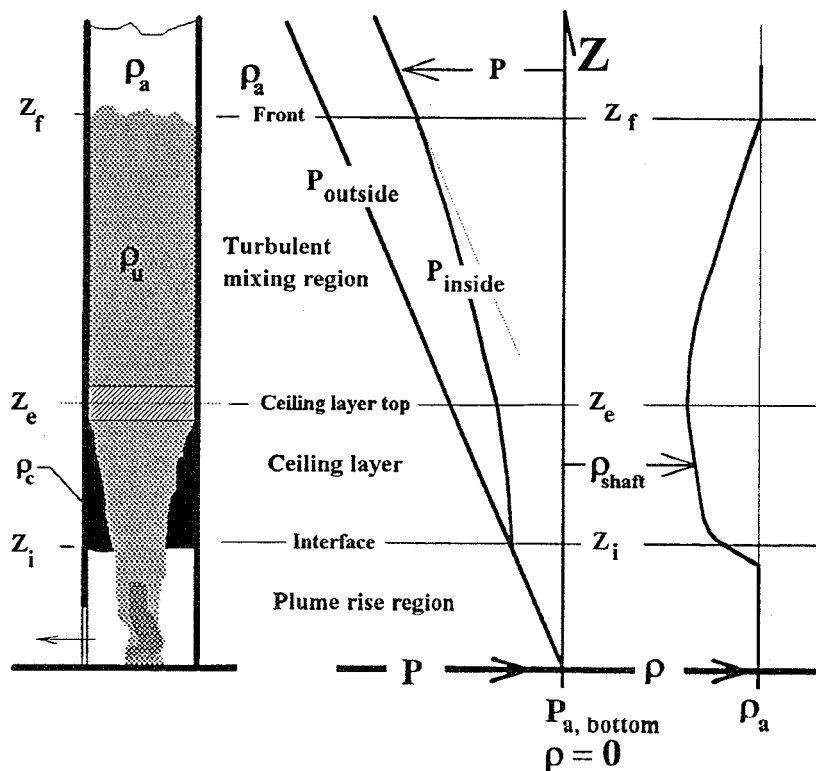
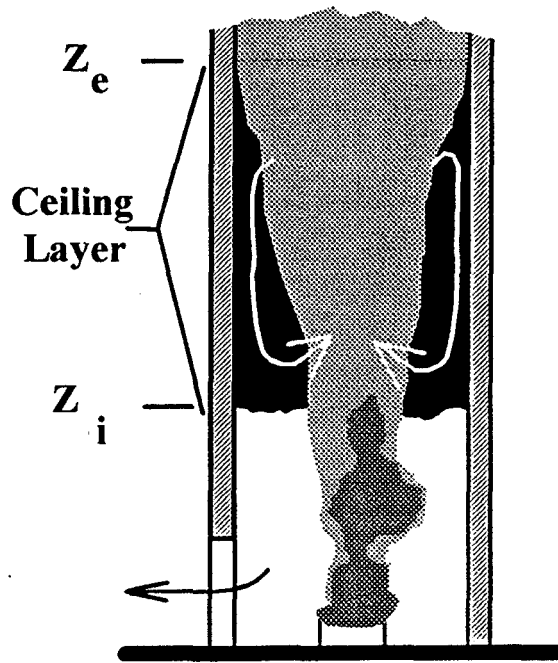


Figure 3. Pressure and Density Distributions in Shaft, See Figure (2C).

In sketch 2(b), the edges of the head of the plume reach the walls of the shaft at an elevation called Z_e and cut off the possibility that gas from above the

plume can flow around the plume and eventually through the door. Consequently, no air from above the plume can now leave the room through the door and the upward motion of the plume gas is blocked. In the space above this Z_e level, mixing between the plume gas and air is no longer controlled by simple plume-rise processes but is fixed by the turbulent mixing process that is associated with the Rayleigh-Taylor instability. This instability occurs in the present context because low-density, hot gas in the plume lies beneath the higher-density, cooler air in the shaft.



After the plume reaches the walls of the shaft, air is still entrained along the sides of the plume (see sketch 2(c) and sketch at left), and this additional gas then returns toward the fire source in the form of a *ceiling layer* whose interface with the cooler air (Z_i in the figure) moves *down* toward the floor.

The development of this ceiling layer proceeds almost as if a porous ceiling were present near the level at which the plumes intersect the side walls at elevation, Z_e . The location of this

front and the rate of energy and mass across this poorly defined boundary control the rate of transport of the gas originally in the shaft toward the exit.

The gas properties in the ceiling layer region are approximately uniform due to the mixing between the plume flow and gas in the ceiling layer. The motion of the interface and the top of the plume are now controlled by different processes.

Finally, in sketch 2(d), we suppose that the window near the top of the shaft breaks and allows the hot gas to communicate with the outside world. Because the average density within the shaft is less than that outside, the rate of decrease of pressure with elevation will be less inside the shaft, (see Figure 3). Consequently, the pressure within the shaft at the window level in Figure 2(d) will be greater than that outside the shaft at the same elevation.

Because the pressure at the window level is higher inside the shaft than outside, hot gas within the shaft will flow out of the window and in general the interfaces at levels Z_e and Z_i will rise within the shaft. The consequences of this flow will affect the entire flow field and, in particular, the levels Z_i , Z_e and Z_f .

Heat transfer from the gas in the shaft to the walls of the shaft is important element in this flow field because heat transfer from the gas changes the buoyancy of the gas, which is the driving force for the turbulent mixing process. Finally, viscous losses at the walls and the development of natural convective flows may also influence the development of the mixing process by damping the turbulent motions of the gas.

Three regions, defined for the flows in both Figure 2 and 3, are illustrated in Figure 3: First, the buoyant plume region, second the ceiling layer region and finally the turbulent mixing region. Both the buoyant plume region and ceiling layer region have been studied in detail and current models may be adequate to describe them when the stack effect is absent. However, interaction of the freely rising plume with the sides of the shaft, the boundary conditions applicable at the interface at level Z_e , and the turbulent mixing processes in the presence of the effects of heat transfer have not been adequately described.

The focus of the work reviewed here is a study of the turbulent mixing region for flows in which the effects of heat transfer were neglected. A description of the flow processes that occur in the turbulent mixing region requires that a model for the turbulent mixing process be developed that will predict the rate of rise of the front at Z_f and the density of the gas below the front. This description includes models for the entrainment rate of the mixing process at the front and the density distribution within the turbulent mixing region. The energy and mass exchange across the interface separating the ceiling layer and the turbulent mixing region, defined schematically in Figures 2 and 3 are not considered here.

In its simplest form, the flow under study involves the motion of a light fluid from a large reservoir upward into a vertical shaft that is open only at its bottom and that is initially filled with a heavier fluid. See the sketch shown in Figure 4.

In much of the work reviewed here, the experiment was carried out as suggested in Figure 4, and the light and heavy fluids were primarily water and a salt-water mixtures with densities from 1 to 10% greater than that of water. However in a few experiments gases with different molecular weights were used. Only a few experiments were carried out in which buoyancy was produced by heating the lighter gas, and the heat transfer effects were not examined in any detail.

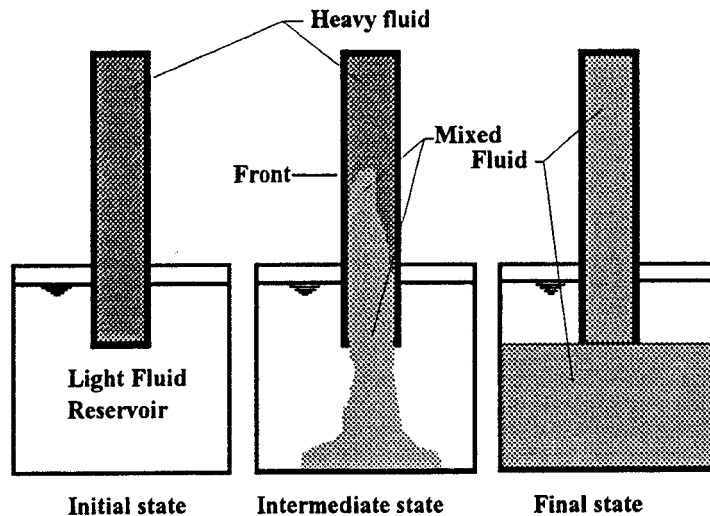


Figure 4. The Problem Examined Experimentally.

A typical experiment started when the bottom of the shaft was suddenly opened and exposed to a large reservoir filled with lighter fluid. The experiment was allowed to continue until the density differences between the ambient fluid and that in the shaft became too small to measure.

This configuration had the advantage that it was clearly defined and was as simple as we could study while still keeping the most important features of real flows with the exception of heat transfer. The aim of the work was to provide the information required for the scaling of the motion of the front of the mixed region, the density profile within the shaft, and the subsequent removal of all of the heavy fluid from the shaft.

The flow configuration for the experimental program is shown in the schematic diagrams in Figures 4. Using a large reservoir of low density as the boundary condition at the bottom of the shaft simplifies the boundary condition at the bottom of the shaft and removes problems involved with the

description of the development of the ceiling layer region discussed above and shown in Figures 2 and 3.

The simple boundary conditions used in these experiments were expected to aid us in developing an understanding of the mixing process. Flows in which the low density fluid is introduced into the shaft by way of a plume and flows with various wall openings such as those described above have not yet been studied in detail.

4. EXPERIMENTAL APPARATUS

The fluids used in most of the experiments reported in Cannon and Zukoski (1976)³ were water and salt-water mixtures. The density of the fluid within the shaft was measured as a function of the time with electric conductivity probes located at various elevations on the centerline of the shafts and the motion of the front was also visualized by dyeing either the salt-water initially in the tube or the ambient water.

The tubes were right circular cylinders and were transparent so that the dye at the front could be followed by eye or with TV cameras. Tubes with diameters from 3.8 to 18 cm and lengths from 29 to 89 diameters long were used in the experiments.

Before the beginning of the experiment, the tubes were filled with the more dense fluid and closed with a thin rubber membrane held under tension. The tubes were held in a vertical position and the mouth of the tube was held under the surface of a large reservoir of fresh water. The experiment was started when the membrane was ruptured and pulled away from the mouth of the tube.

The effect of the initial disturbance caused by the rupture of the membrane was not thought to strongly influence the experimental results except in the first few diameters of the shaft and was ignored in the analysis of the data.

Density measurements were made with standard hydrometers that were used as the primary standards to calibrate electrical conductivity measurements. The latter data were then used to obtain the density of the salt water mixtures through a second calibration.

³ Cannon, Jonnie. B. and Zukoski, Edward. E., (1975), *Turbulent Mixing in Vertical Shafts Under Conditions Applicable to Fires in High Rise Buildings*, Technical Fire Report No. 1 to the National Science Foundation, California Institute of Technology, Pasadena, California.

5. MODELING

Analysis of the Basic Problem: The analysis of the results was based on dimensional considerations and a simple estimate of the turbulence produced by the positive density gradient in the tube. The notation used in the following analysis is shown in the left hand side of the sketch in Figure 5. Here ρ_i and ρ_a are the initial density within the tube or shaft and the density in the ambient or reservoir fluid at the bottom of the shaft..

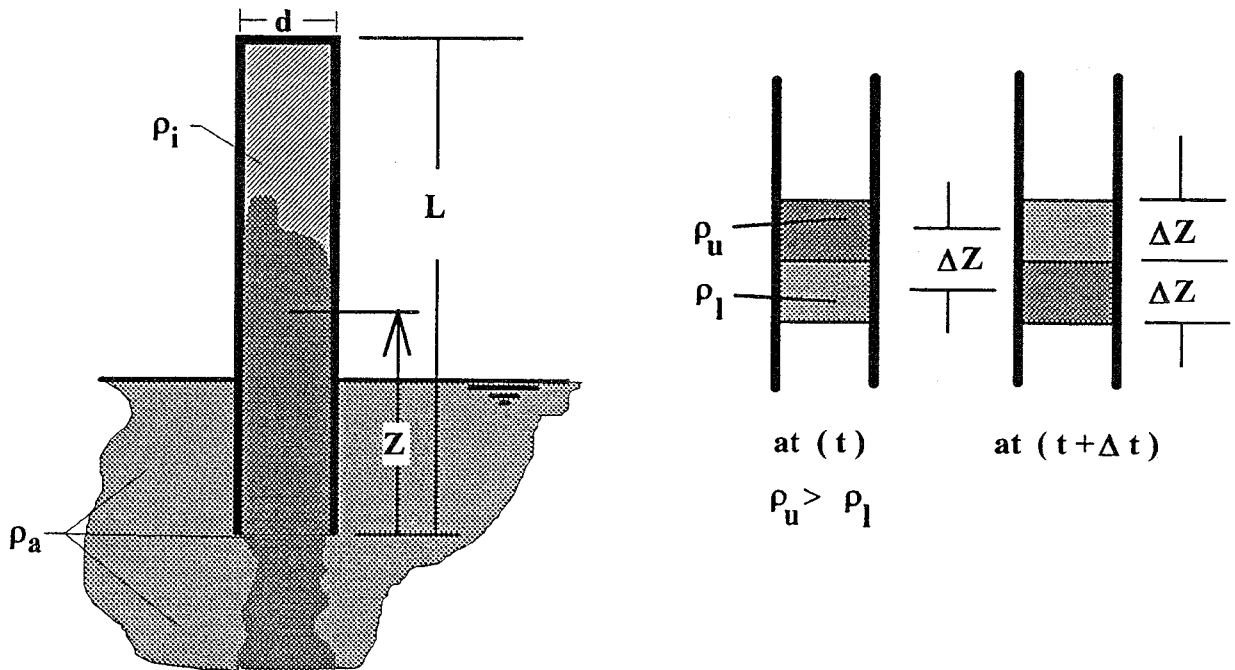


Figure 5. Sketch Defining Notation for the Analysis.

The analysis depended on several restrictive approximations. The most important of these were that:

1. the viscosity of the fluids were ignored.
2. the fluid was treated with the Boussinesq approximation that ignores density variations except when the density difference is considered.

3. the density at the bottom of the shaft, $\rho\{Z = 0, t\}$ was taken to be the ambient density, ρ_a . A better assumption here would probably be to place this condition at a point at least one diameter, d , below the bottom of the shaft.

and

4. the shafts were all right circular cylinders.

Two phases of the experiment must be analyzed here. In the first, the front of the disturbance propagates up the tube and reaches the top at $t = t_0$. In the second, the density distribution in the tube changes with time until the density difference, between fluid within the tube and the ambient value, becomes very small throughout the tube. In the following paragraphs, we first describe a simple model for the turbulent mixing process and then apply this result to compute the flows generated by several geometric configurations of shafts and reservoirs.

Turbulent Diffusion Model: The basic idea used in the analysis is to assume that the molecular diffusivity is negligible, a most reasonable idea, and that the turbulent diffusivity is given by the product of a velocity fluctuation w' and a length scale λ . The value for w' is determined from an energy balance, see right hand side of Figure 5, based on the potential energy released when a mass of fluid with a vertical scale ΔZ and with density ρ_u moves downward in the shaft and displaces a mass with the same scale but a smaller density, ρ_l . Here we assume that $\rho_u > \rho_l$. The value for w' is then calculated using the idea that the change in potential energy between the two configurations appears as the kinetic energy of the fluctuations:

$$\rho (w')^2 \propto (\rho_u - \rho_l) g \Delta Z \quad \text{and} \quad (\rho_u - \rho_l) \approx \left(\frac{\partial \rho}{\partial Z} \right) \Delta Z$$

Thus,

$$w' \propto \sqrt{\frac{1}{\rho} \left(\frac{\partial \rho}{\partial Z} \right) g (\Delta Z)^2}$$

The turbulent diffusivity is then estimated from the product of w' and an appropriate scale length, λ , to give

$$D_t \equiv w' \lambda \propto \sqrt{\frac{1}{\rho} \left(\frac{\partial \rho}{\partial Z} \right) g} (\Delta Z) \lambda$$

The most natural selection for ΔZ and λ is the tube diameter, d . However, the experimental results are best fit by making:

$$(\Delta Z) \lambda \propto [(d)^7 L]^{1/4} = d^2 \left(\frac{L}{d} \right)^{1/4}$$

where L is the length of the tube. The dependence of the turbulent diffusivity on the length of the tube was unexpected and still has not been resolved to our satisfaction. However, it may be due to the neglect of the convective transport terms in the differential form of the continuity equation discussed below.

The final approximation involves using the Boussinesq approximation that the density that appears in the denominator of the diffusivity equation can be taken to be the ambient density. This does not cause great problems for the water/salt-water modeling, but probably will for a hot/cold gas model.

However, if we use these results and approximations, the final form for the diffusivity is

$$D_t \propto \sqrt{\frac{1}{\rho_a} \left(\frac{\partial \rho}{\partial Z} \right) g} d^2 \left(\frac{L}{d} \right)^{1/4} \quad (5)$$

and the proportionality constant must be determined from experimental results.

For the water/salt-water modeling work, the assumption that $(\rho \approx \rho_a)$ in the above equation is a good approximation. Given this assumption, the mean velocity of the fluid in the shaft can be shown to be small. When the convective transport is neglected, the continuity equation becomes:

$$\frac{\partial \rho}{\partial t} = \frac{\partial}{\partial Z} \left(\int_t \frac{\partial \rho}{\partial Z} \right)$$

and therefore is reduced to

$$\frac{\partial \rho}{\partial t} \propto \left[\sqrt{\frac{g d^4}{\rho_a}} \left(\frac{L}{d} \right)^{\frac{1}{4}} \right] \left(\frac{\partial \rho}{\partial Z} \right)^{\frac{3}{2}} \quad (6)$$

in which the square bracketed term is a constant for a given experiment.

If we define the dimensionless parameters,

$$Z/L = X, \quad [(\rho - \rho_a)/(\rho_i - \rho_a)] \equiv \theta, \quad \text{and} \quad \tau = \left(\sqrt{\frac{\Delta \rho_i g}{\rho_a d}} \left(\frac{L}{d} \right)^{\frac{9}{4}} \right) t,$$

the approximate continuity equation becomes:

$$\frac{\partial \theta}{\partial t} = k \frac{\partial}{\partial X} \left(\frac{\partial \theta}{\partial X} \right)^{\frac{3}{2}} \quad (7)$$

This form will now be used to examine a number of flow configurations in the following paragraphs.

Here, k is the constant of proportionality for the diffusion equation. Note that the nonlinear dependence on the gradient of density in Equation 7 indicates that a wave like front can be present even though the flow is dominated by a diffusive process.

Equation 7 can be solved by the separation of variables and the solution put in the form: $\theta \equiv H\{\tau\} F\{x\}$.

We find that:

$$\frac{1}{(H)^{\frac{3}{2}}} \frac{dH}{dt} = \left(\frac{3k}{2F} \right) \sqrt{\frac{dF}{dx}} \frac{d^2 F}{dx^2} = -\alpha$$

and consequently that:

$$H\{\tau\} = \frac{1}{[A + \alpha(\tau - \tau_0)]^2}$$

in which A is a constant. A first integral for F gives:

$$\frac{dF}{dx} \equiv \left(B - \left(\frac{5}{6}\right) \left(\frac{\alpha}{k}\right) F^2 \right)^{\frac{2}{5}}$$

A numerical solution for F{x} is usually necessary.

Density changes in a shaft after the front reaches the top of the shaft:

We assume that the front of the mixing region reaches the top of the shaft at $t = t_0$. For the simple shaft problem illustrated in Figures 4 and 5, the boundary at times after t_0 are:

$$\theta\{\tau, x\} = 0 \quad \text{at } x = 0 \quad \text{and} \quad \left(\frac{\partial\theta}{\partial X}\right) = 0 \quad \text{at } x = 1$$

In terms of the functions H and F these conditions become:

$$\text{At } x = 0: F\{x\} = 0$$

$$\text{At } x = 1: F\{x\} = 1 \quad \text{and} \quad \left(\frac{\partial F}{\partial x}\right) = 0$$

$$\text{At } \tau = \tau_0, H\{\tau\} = 1$$

Application of the boundary conditions leads to the solutions:

$$H\{\tau\} = \frac{1}{[1 + \alpha(\tau - \tau_0)]^2} \tag{8a}$$

and

$$\frac{dF}{dx} \equiv \left(\frac{5}{6} \frac{\alpha}{k} \right)^{\frac{2}{5}} (1-F^2)^{\frac{2}{5}} \quad (8b)$$

A numerical solution for $F\{x\}$, defined by Equation 8b, is shown in Figure 6 with experimental data discussed in a later section. A close approximation to this numerical solution can be put in simple algebraic form:

$$F\{x\} \approx \left(1 - (1-x)^{\frac{3}{2}} \right) \quad (9a)$$

Thus, for the basic configuration:

$$\theta = \frac{F\{x\}}{[\alpha(\tau - \tau_0) + 1]^2} \approx \frac{\left(1 - (1-x)^{\frac{3}{2}} \right)}{[\alpha(\tau - \tau_0) + 1]^2} \quad (9b)$$

This solution depends on the value for the ratio (α/k) which was found from analysis to be about 2.72 for the geometric configuration studied here.

A consequence of the solution obtained here is the separation of the dependence on time and elevation in the tube. For example:

$$\sqrt{\frac{\theta\{x,t\}}{F\{x\}}} = \frac{1}{[\alpha(\tau - \tau_0) + 1]} \quad (10a)$$

$$\text{and } \therefore \text{ since } \theta \equiv \frac{(\rho - \rho_a)}{(\rho_i - \rho_a)} \equiv \frac{(\Delta\rho)}{(\Delta\rho_i)}$$

$$\sqrt{\frac{(\Delta\rho_i)}{(\Delta\rho\{x,\tau\})} F\{x\}} = [\alpha(\tau - \tau_0) + 1] \quad (10b)$$

Thus, this model predicts that the term on the left hand side of Equations 10a and 10b must depend linearly on the time after the mixing region reaches the top of the tube.

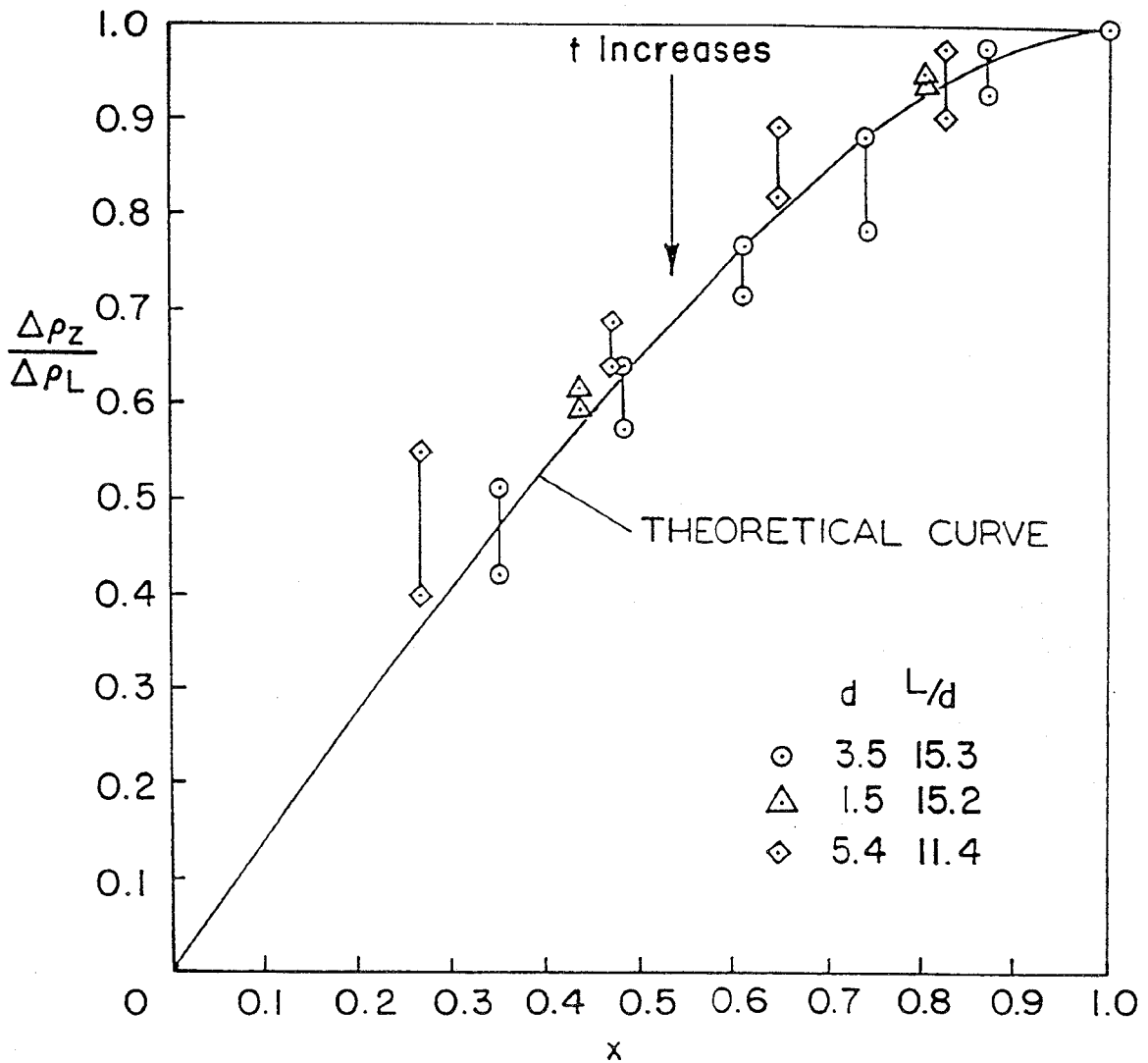


Figure 6. Density Distribution Function $F\{x\}$ for Configuration of Figure 5 and 7(A).

Finite Reservoir Problems for $t > t_0$: Several other problems can be solved with this approximate solution by changing the boundary conditions. The most easily changed parameter involves the boundary conditions at the bottom or top of the shaft and the problems to be solved are illustrated in Figure 7:

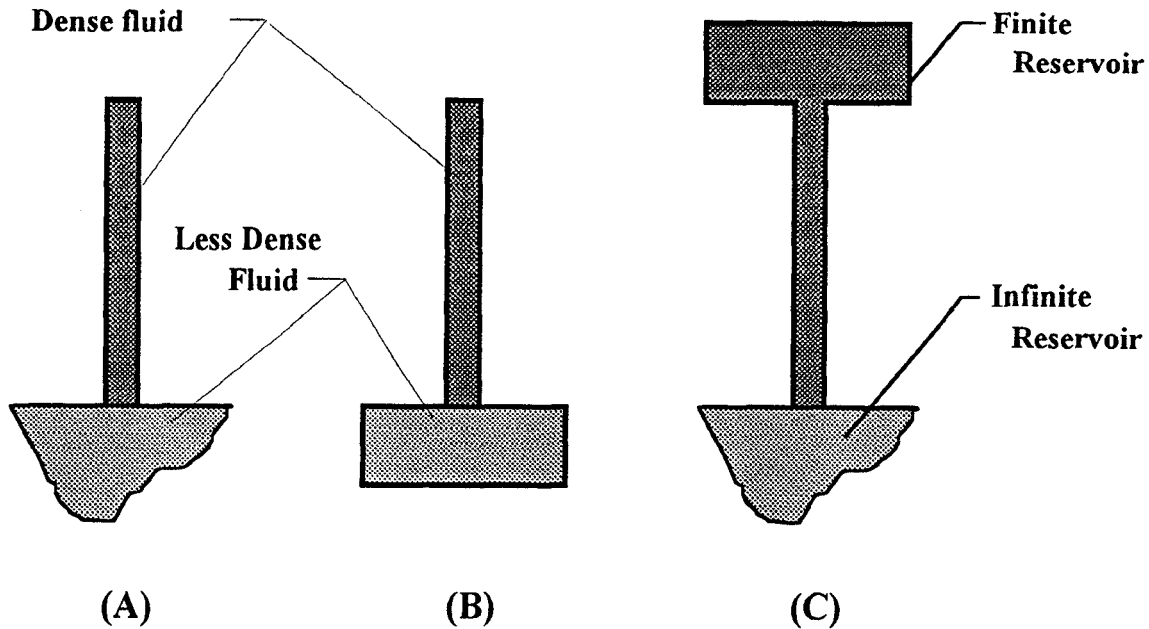


Figure 7. Initial Conditions for Configurations with Finite Reservoir Volumes. (A) The basic problem with an infinite reservoir at bottom of shaft, (B) finite reservoir at bottom of shaft, and (C) finite reservoir at top of shaft and infinite reservoir at bottom.

In the left hand sketch, 7 (A), the volume of the reservoir beneath the shaft is infinite. In sketch 7 (B), a finite reservoir replaces the infinite reservoir at the bottom of shaft. Experiments and calculations have been carried out with this configuration with the volume of the reservoir ranging from 2 to 24 times that of the shaft. Only calculations were performed for the configuration shown in sketch 7 (C).

The assumption made for the finite size reservoirs is that they can be treated as a homogeneous or perfectly region with uniform density. This simple boundary condition for the bottom or top of the shaft is now a function of the

time. This condition is applied at the exit of a shaft next to the reservoir and can be written in terms of the cross section of the shaft A_p as:

$$A_p \mathcal{D}_t \left(\frac{\partial \rho}{\partial Z} \right)_{\text{exit}} = (V_{\text{reservoir}}) \left(\frac{\partial \rho}{\partial t} \right)_{\text{reservoir}} \quad (11)$$

The ratio of the volume of the finite sized reservoir to the volume of the shaft, $V_r \equiv (V_{\text{reservoir}} / V_{\text{shaft}})$, now appears in the solutions because the volume of the reservoir appears in this boundary condition. When the separation of variable solution described above is applied again here, the differential equation for $\theta \{x, \tau\}$ and result for $H\{t\}$ is as before in Equations 8 and 9. The equation for $F\{x\}$ in Configuration 7(C) becomes:

$$\left(\frac{dF}{dx} \right) = \left(\frac{5\alpha}{6k} \right)^{\frac{2}{5}} (C - F^2)^{\frac{2}{5}}$$

Here, C is a constant. The boundary conditions become:

$$\left. \left(\frac{dF}{dx} \right) \right|_{x=1} = \left(\frac{\alpha}{k} \right) \left(\frac{1}{V_r} \right) \quad \text{and}$$

$$F\{x\} = 0 \quad \text{at } x = 0 \quad \text{and} \quad F = 1 \quad \text{at } x = 1.$$

Both $F\{x\}$ and (α/k) now depend on V_r . The solution again has the form:

$$\theta \equiv \frac{\Delta \rho \{x, \tau\}}{\Delta \rho_i} = \frac{F\{x\}}{[\alpha (\tau - \tau_0) + 1]^2}$$

The dependence of (α/k) on V_r and the form for $F\{x\}$ are shown for the problem in 5(C) in Figures 8a and 8b. Here, $V_r = \infty$ corresponds to the basic problem. The reservoirs make surprising little difference for this configuration until V_r is near 1.0.

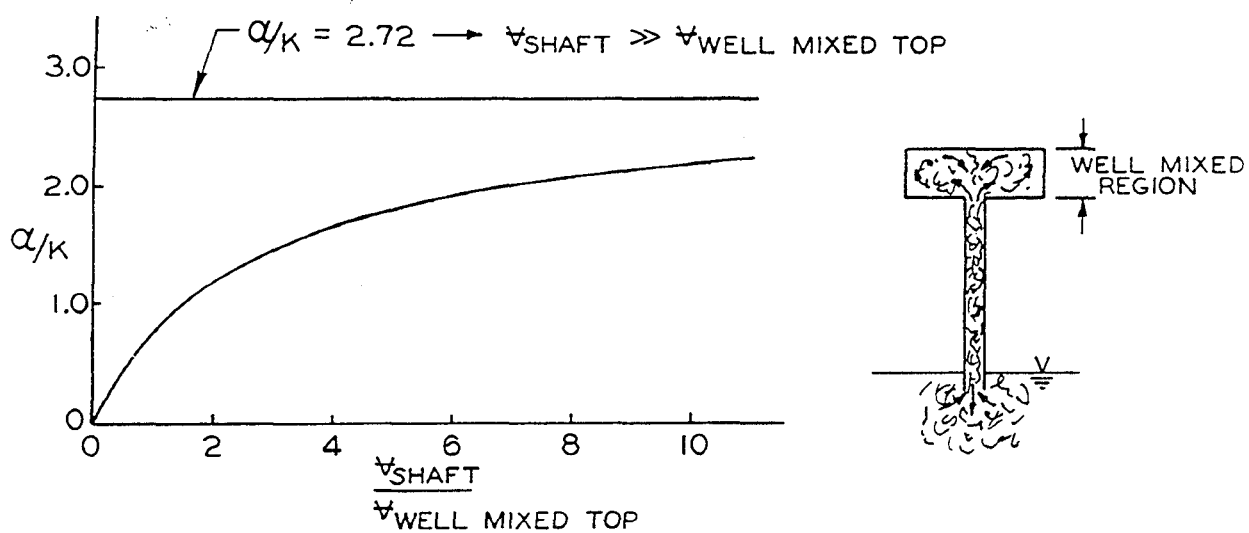


Figure 8a. Values of (α/k) versus V_r for Configuration 7(C).

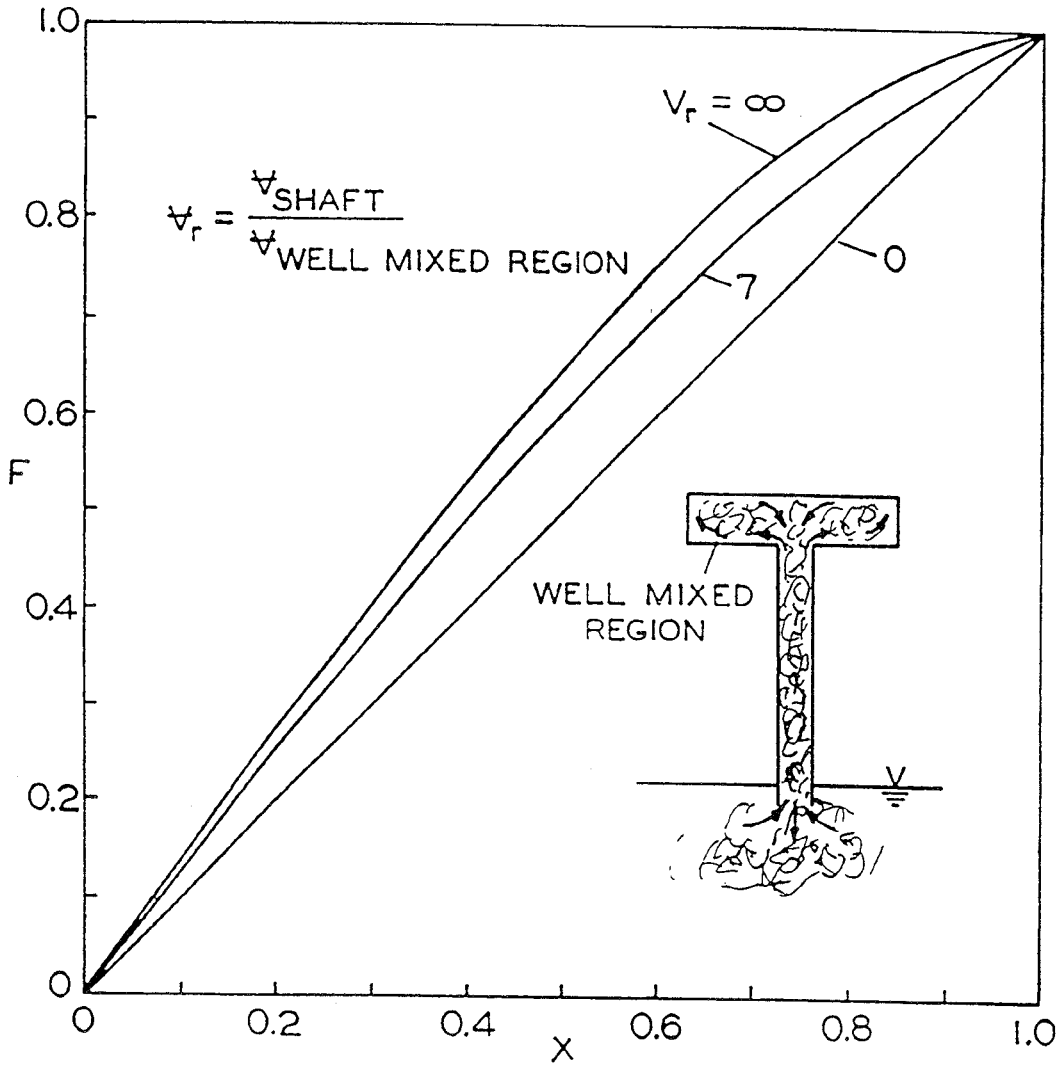


Figure 8b. Density Distribution Function $F\{x\}$ for Configuration 7(C).

Solutions for the configuration 5 (B) were obtained in a similar manner and are shown in Figure 9a and 9b. Again, V_r makes a difference only when the $V_r < 3$.

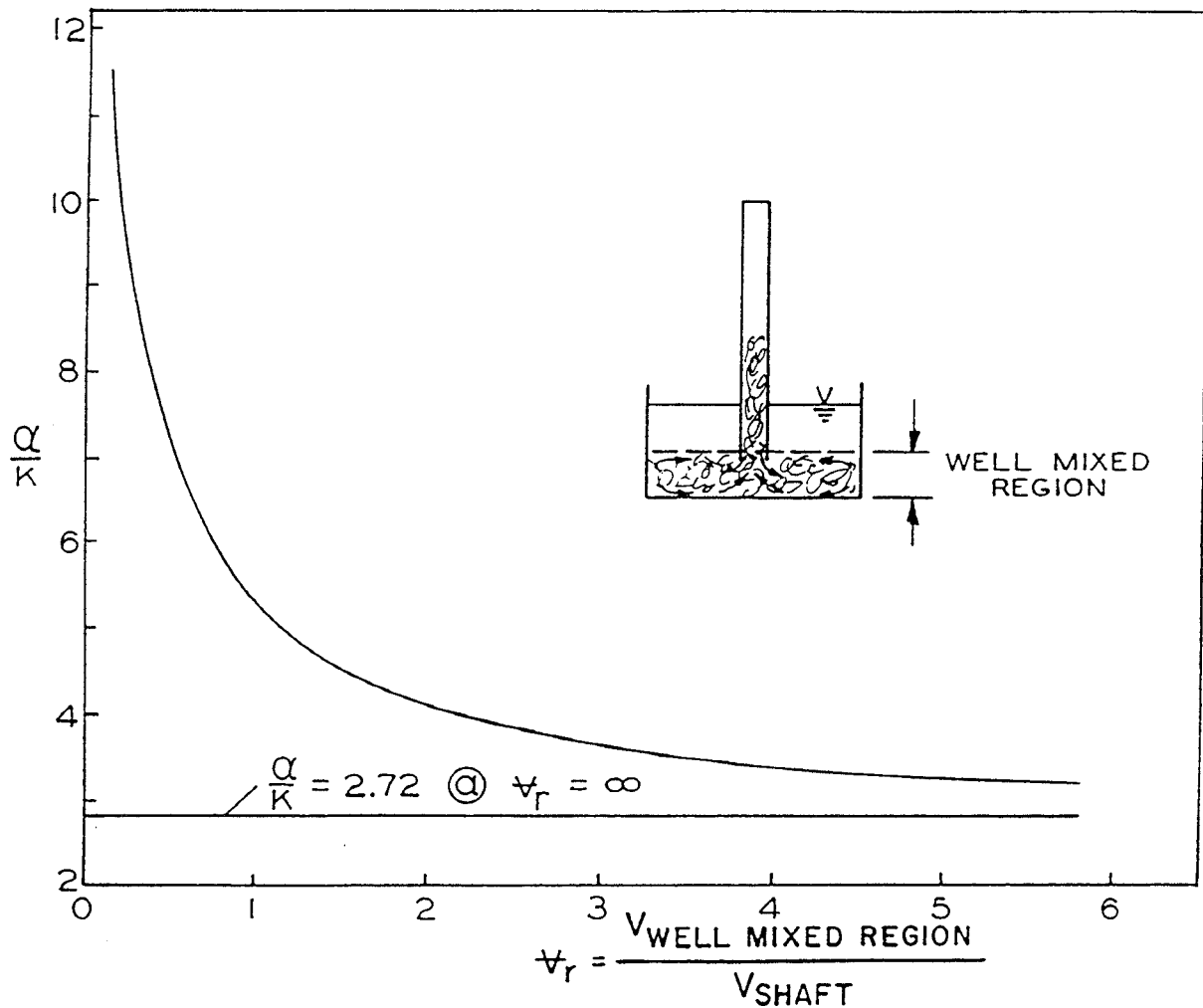


Figure 9a. Values of (α/k) for Configuration of Figure 7(B).

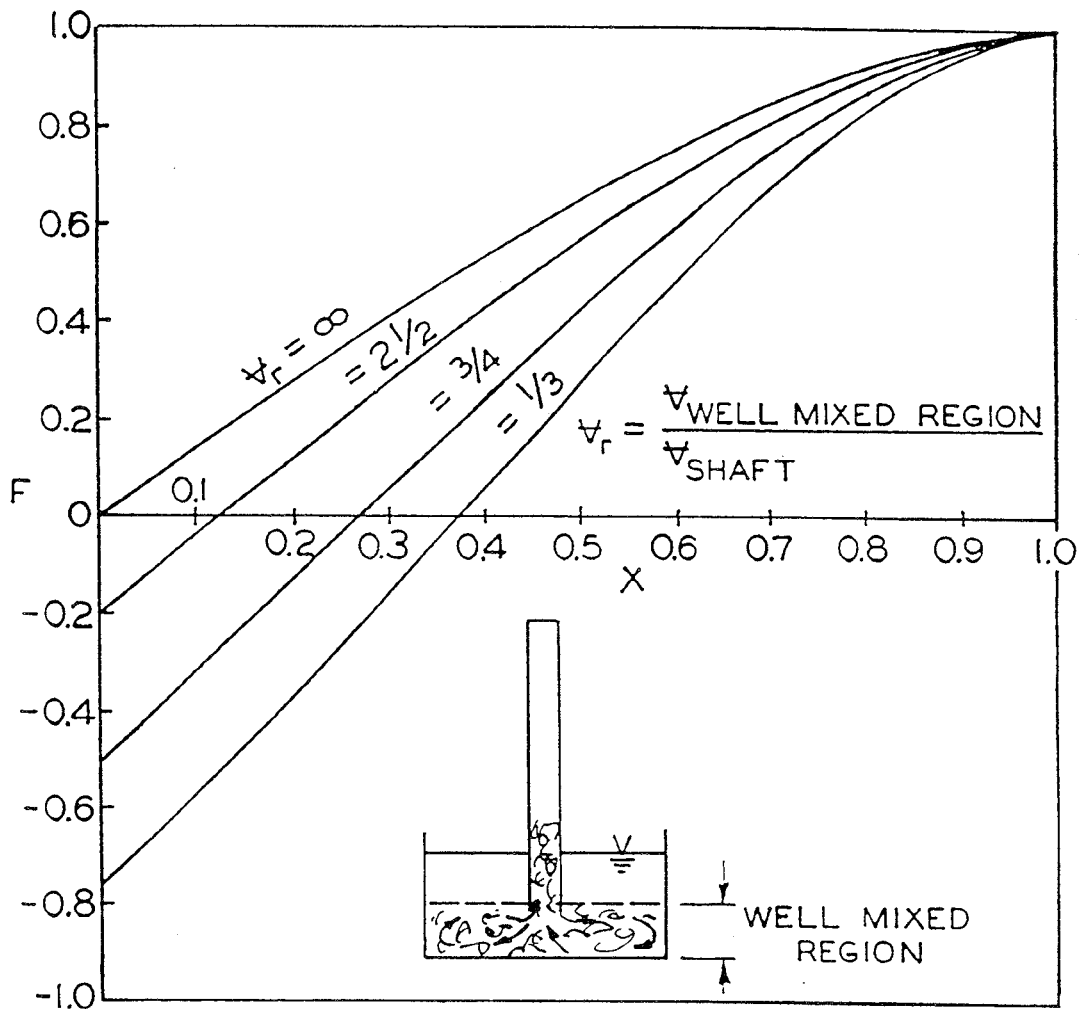


Figure 9b. Density Distribution Function $F\{x\}$ for Configuration 7(B)

Density changes in a simple shaft for ($0 < t < t_0$): The problem here is to calculate the motion of the front of the turbulent mixing region as it propagates up the shaft. First, Equation (5) is modified by changing the dependence on the length from L to Z_f where Z_f is the location of the front. This exchange gives:

$$D_t \propto \sqrt{\frac{1}{\rho_a} \left(\frac{\partial \rho}{\partial Z} \right) g} d^2 \left(\frac{Z_f}{d} \right)^{\frac{1}{4}}$$

and the corresponding form for Equation 7 is then:

$$\frac{\partial \theta}{\partial \tau'} = k (x'_f)^{\frac{1}{4}} \frac{\partial}{\partial x'} \left(\frac{\partial \theta}{\partial x'} \right)^{\frac{3}{2}} \quad (12)$$

Where: $x'_f \equiv Z_f / d$, $x' \equiv Z / d$, $\tau' \equiv \sqrt{\frac{g \Delta \rho}{d \rho_a}} t$

The boundary conditions are that: $\theta \{x'_f, \tau'\} = 1.0$ and $\left. \frac{\partial \theta}{\partial x'} \right|_{x'_f} = 0$

This equation is integrated with the aid of an integral technique based on the form for F used in the successful representation for the basic problem:

$$\theta \{x', \tau'\} = \left[1 - \left(1 - \frac{x \{ \tau' \}}{x'_f \{ \tau' \}} \right)^2 \right] \quad (13)$$

The solution indicates that τ' is the correct correlation parameter and that

$x'_f \propto (\tau')^{\frac{4}{5}}$. Unfortunately the experiments suggest that the power should be nearer 0.60 than 0.44. Thus, the model for the spreading process is not useful. (Certainly, a more general approach than that suggested by the use of Equation 13 needs to be made here.)

6. Experimental Results

The results of experiments carried out with the water/salt-water modeling technique and described in the report by Cannon and Zukoski ⁴ will be discussed here.

Motion of the Front in a Simple Shaft: The motion of the front made visible by dyeing the ambient fluid was irregular and appeared to be the result of waves of turbulence that originated at the exit of the shaft. They subsequently propagated up to and pass beyond the front, and propelled the front into the unmixed fluid at the top of the shaft. Fingers of mixed fluid frequently moved several diameters up one side of the shaft and then fell back to completely fill the tube with mixed fluid.

The data for the location of the front as a function of time shown in Figure 10 for a range of values for the shaft diameter, d , and length, L . The data are correlated by the expression:

$$\frac{Z_f}{d} = (0.97) \left[\sqrt{\frac{\Delta\rho_i g}{\rho_a d}} t \right]^{0.57} \quad (14)$$

The correlation improves as the distance from the open end of the shaft increases and the weak scatter of the data for the 6 fold increase in diameter suggests that viscous effects are not important.

Because the data correlation by Equation 14 is very good, the proposed scaling parameters for the elevation and time appear to be appropriate scaling parameters although the power law is different from that suggested by the model. Given the differences between computed and experimental results, the application of this empirically derived model to fire flows, even when heat transfer is not a dominant feature, should be made with caution.

⁴ Cannon, Jonnie. B. and Zukoski, Edward. E., (1975), *Turbulent Mixing in Vertical Shafts Under Conditions Applicable to Fires in High Rise Buildings*, Technical Fire Report No. 1 to the National Science Foundation, California Institute of Technology, Pasadena, California.

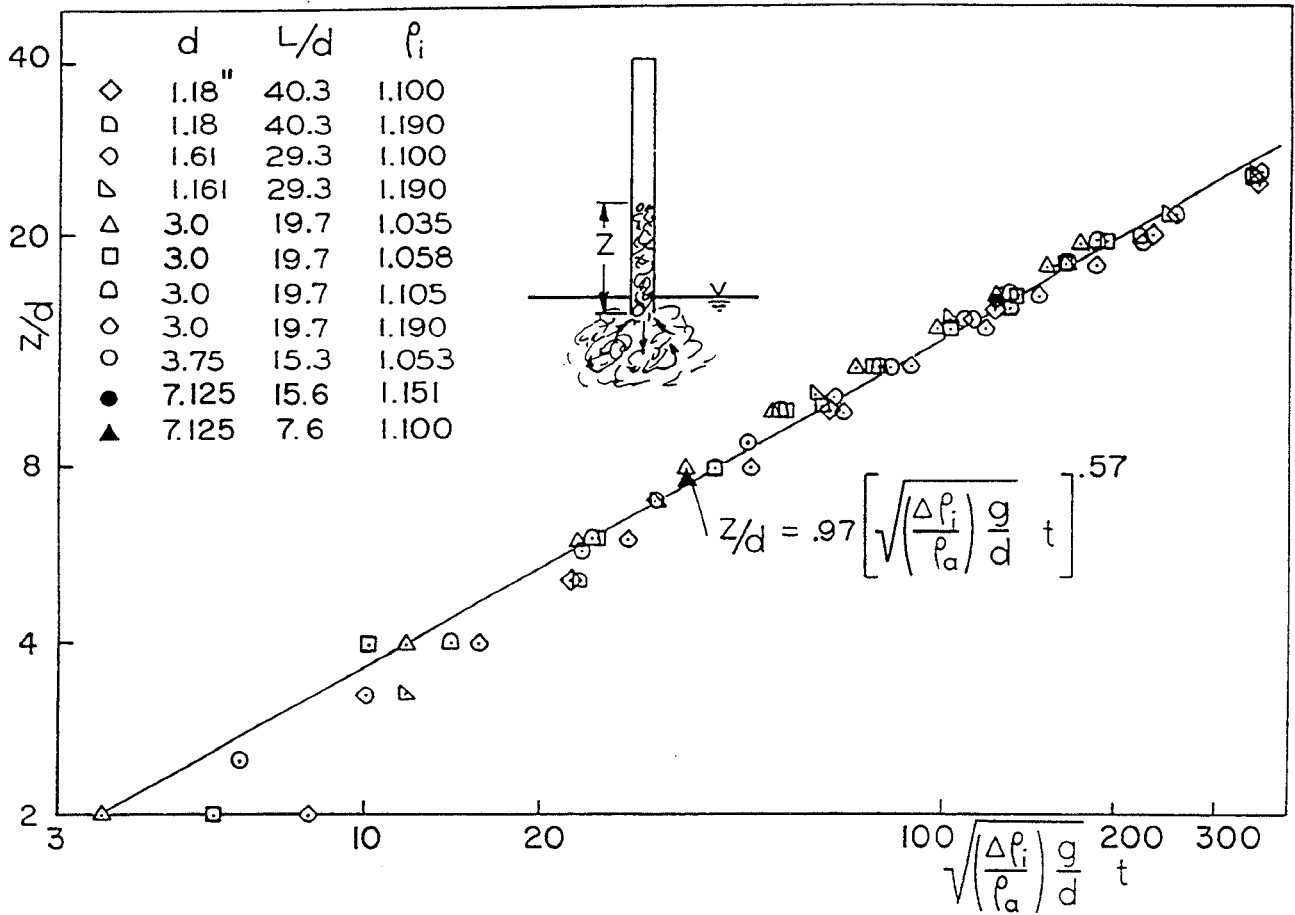


Figure 10. Elevation of the Front as a Function of the Time

Example 3. As an example of the use of Equation 13, return to the problem discussed earlier involving a 30 m shaft with a width of about 3.2 m and with $(\Delta\rho_i / \rho_a) = 0.25$. The turbulent front will move up the shaft in about 66 s compared with the 50 s required for the stack effect example with a similar geometry that was discussed in Example 1 of Section 1. However note that in the stack effect problem, gas with the full density jump is delivered to the window area in 50 s; here, the front of the turbulent mixing region arrives in a comparable time, but substantial density changes will arrive later.

Density Distribution for $t > t_0$ in a Simple Shaft: The dependence of the density profile function $F\{x\}$ on $x \equiv (Z/L)$ is shown in Figure 6 for a few examples and the agreement between data and prediction is good. However, the measured values do change with time and do deviate from the predicted values for the $L/d = 5$ example.

In Figure 11a the square root of the density ratio, $(\Delta\rho_i / \Delta\rho)$ is shown as a function of the dimensionless time for 6 positions within a 9.5 cm shaft. In Figure 11b the same data is shown as the square root of the function $([F\{x\} \Delta\rho_i] / \Delta\rho\{x, \tau\})$.

The separation of variable solution, see Equation 9 and 10 reproduced here, indicates that in general for this flow the density difference at $(Z/L) = x$ and at the top of the shaft, where $x = 1$ and $F = 1.0$ could be written as:

$$\sqrt{F\{x\} \left(\frac{\Delta\rho_i}{\Delta\rho\{x, \tau\}} \right)} = (1 + \alpha [\tau - \tau_0]) \quad \text{and} \quad \sqrt{\left(\frac{\Delta\rho_i}{\Delta\rho\{x=1, \tau\}} \right)} = (1 + \alpha [\tau - \tau_0])$$

Thus, the square root of the reciprocal of density difference ratio, the left side of in these two equations, should be linear functions of time.

This stringent prediction that is tested against the experimental results in Figures 11. In Figure 11a, the data are presented as a function of the reduced time but without including the function $F\{x\}$ as required in Equation 10a, shown on the left side above. At any given elevation the data are linear as required by the model after the front reaches the top of the shaft.

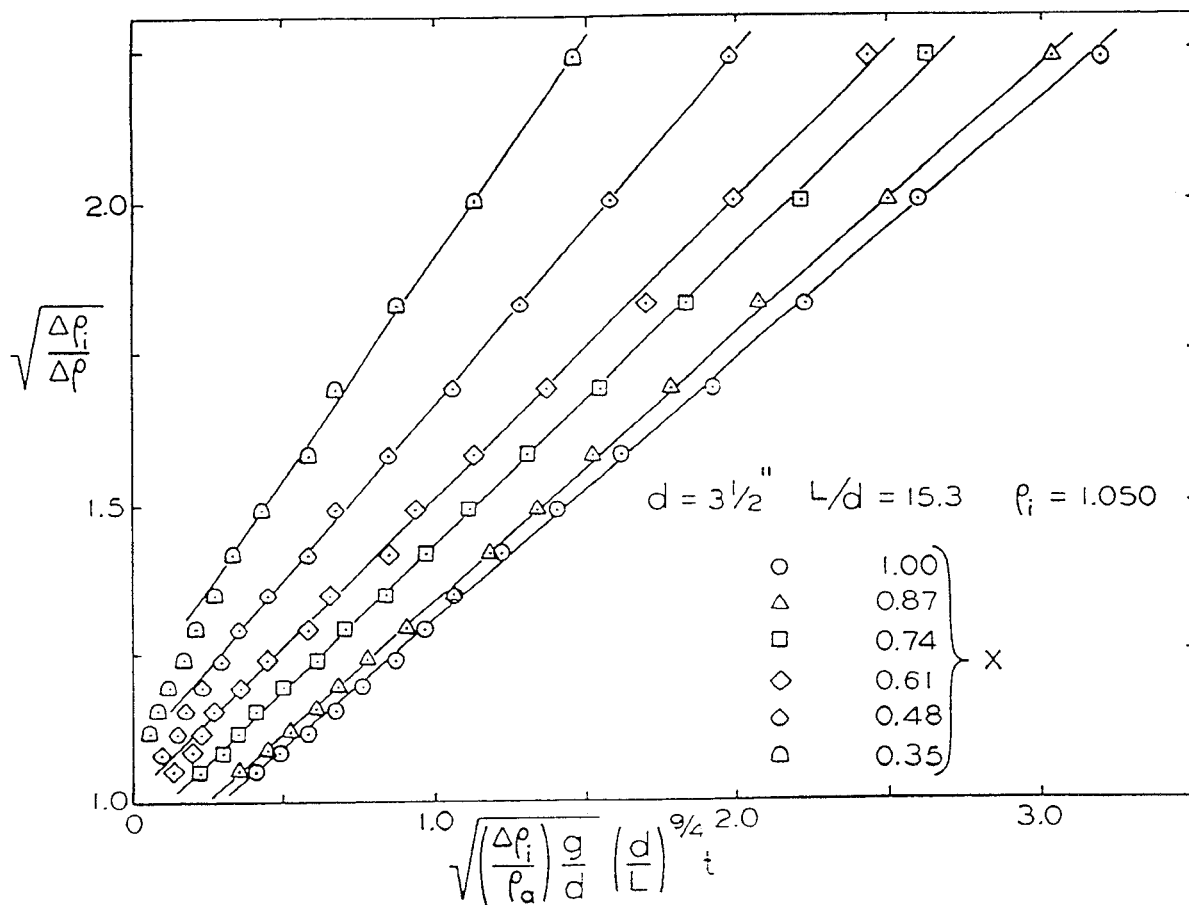


Figure 11a. Dependence of Density-Difference Ratio on Reduced Time.

When the function $F\{x\}$ is included, the correlation of the data, shown in Figure 11b, is excellent at any given value of the reduced time and are a linear function of τ , the reduced time, after the front of the turbulent mixing region reaches the top of the shaft. This good agreement gives confidence in the general structure of the computations leading to equations 10a and 10b.

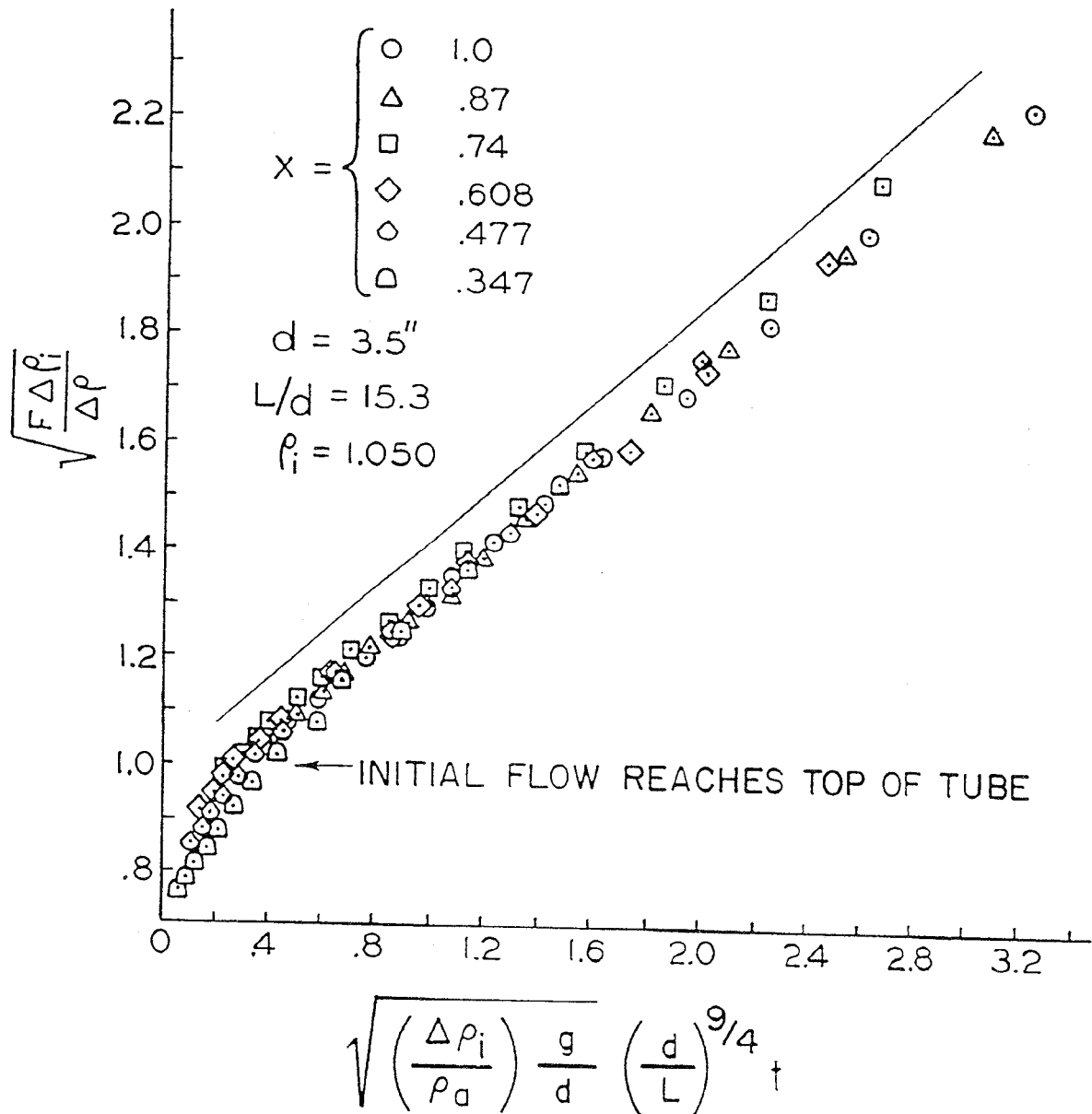


Figure 11b. Normalized Density Ratio for Data of Figure 11a.

Similar data are shown in Figure 12 for the density difference ratio measured at the top of the shaft and for a range of values for d and L . Again the data are linear as required by equation 10 and are well correlated.

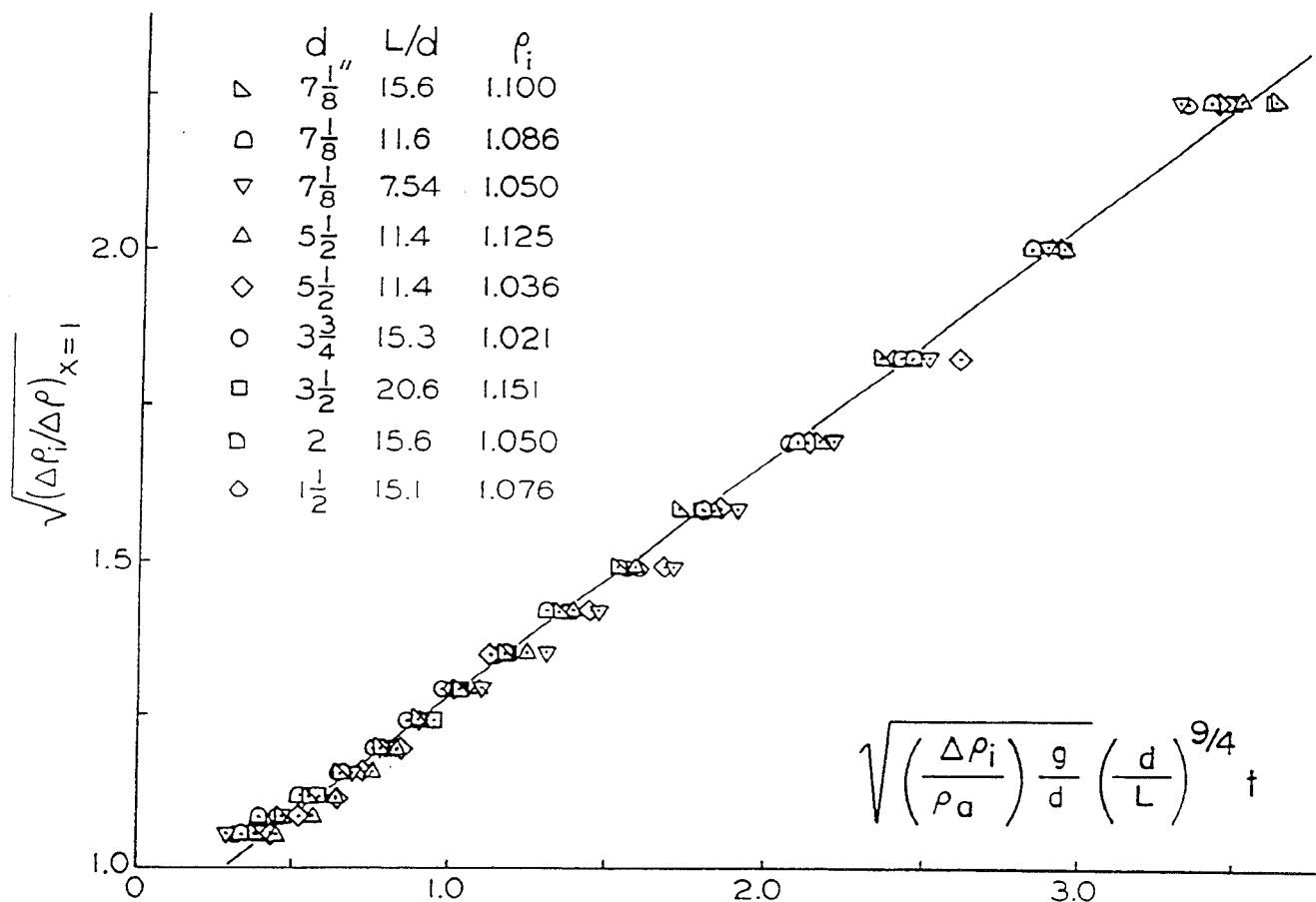


Figure 12.. Normalized Density Ratio for Range of Initial Conditions and Shaft Geometry

Data from the few experiments in which gas mixtures were used to obtain the density differences are shown in Figure 13, and the same general results are obtained although the data for the higher density ratio are offset from those with density ratio less than one.

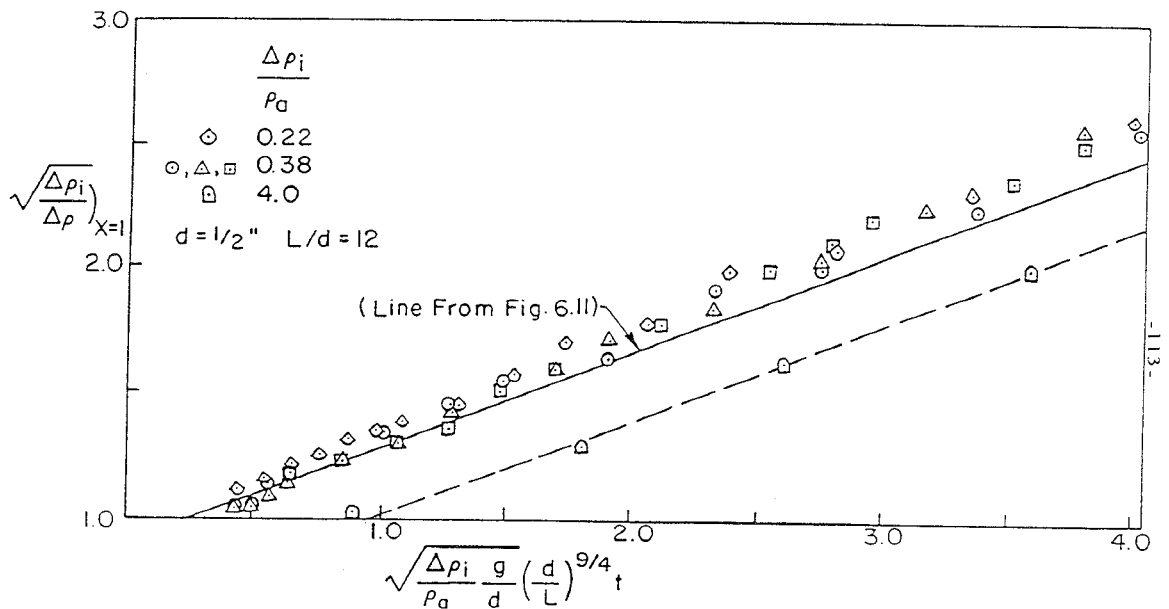


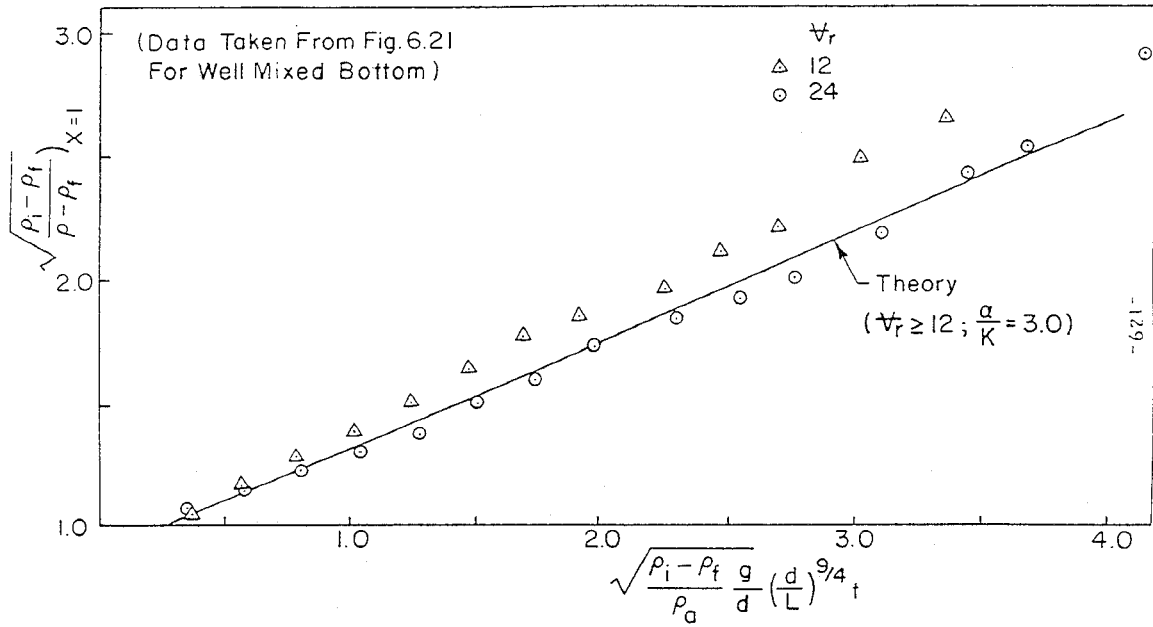
Figure 13. Normalized Density Profile for Gas-based Experiments

Example 4. For an example, return to the problem discussed at the end of the last subsection. The time required for the density difference at the top of the shaft, $\Delta\rho\{x=1.0, t\}$ to reduced to half of the initial density difference, $\Delta\rho_i$, is given by:

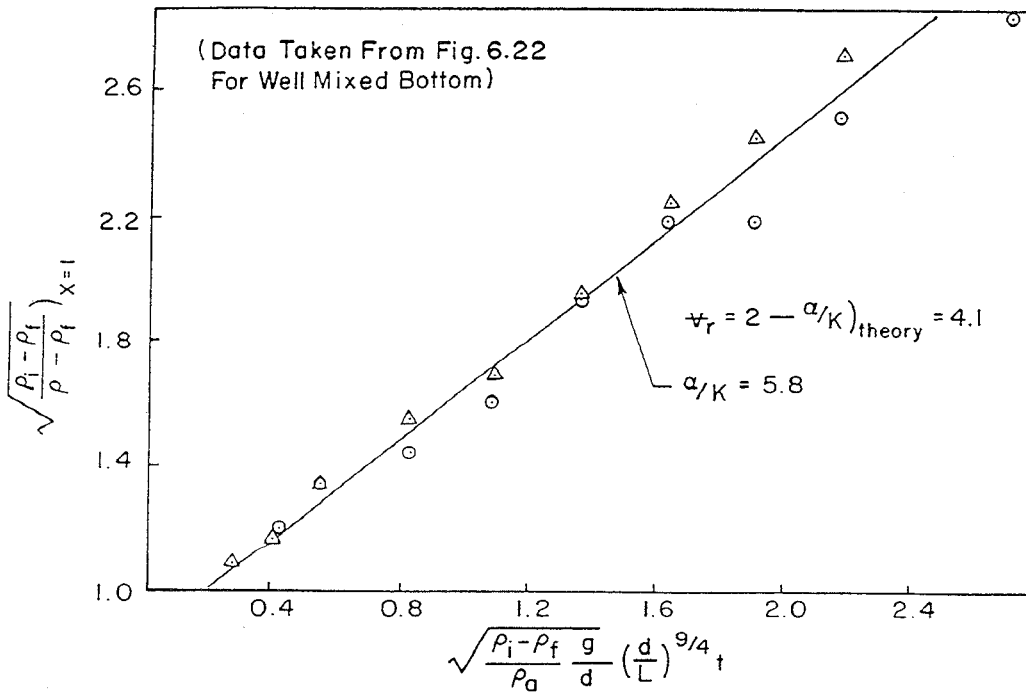
$$t\{ \Delta\rho \{x=1, \tau \} \equiv 0.5(\Delta\rho_i) \} \approx (3.0) \left[\left(\frac{L}{d} \right)^{\frac{9}{4}} \sqrt{ \left(\frac{d}{g} \frac{\rho_a}{\Delta\rho_i} \right) } \right]$$

Here, the constant 3.0 is taken from the data and corresponds to $(\Delta\rho / \Delta\rho_i) = 0.5$. For the current example, with $L/d = 10$, $d = 3.2$ m, $\Delta\rho_i = 0.25 \rho_a$, the time is about 600 s. Thus, although the arrival time of the front of the turbulent mixing region is comparable to that for the stack effect with a large window, the delivery of gas with a substantially different density to the top of the shaft is slower.

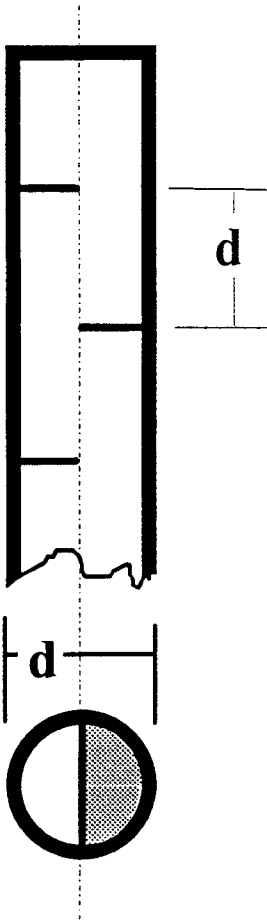
Finite Reservoir Problems for $t > t_0$: Three examples of data obtained with a finite reservoir volumes at the bottom of the shaft, Configuration 7(B), are shown in Figures 14 and 15 for volume ratios 2, 12 and 24. The general form of the solutions is again in agreement with our predictions. The value for the ratio (α / k) that best fits the data is in good agreement with the predicted value for V_r values 12 and 24 but is less satisfactory for V_r of 2.



14. Normalized Density Profile for Finite Volume Reservoir at Bottom of a Shaft.



15. Normalized Density Profile for Finite Volume Reservoir at Bottom of a Shaft..



Stairway Model: Finally, a set of experiments was carried out with a very simple model of a stairway, shown in the sketch at left. The model was made up of a 9.5 cm diameter shaft with an L/d of 7.9 and with semicircular baffles spaced one diameter apart and placed alternatively on opposite sides of the shaft as indicated in the sketch.

In these experiments, flow visualization suggested that a vortex like motion was established in the space bounded by two adjacent baffles and that the transport of mixed fluid up into the next level was greatly delayed.

The effect of the baffles is shown in Figure 16 as a plot of the density-difference ratio at the top of the shaft versus the reduced time. Note that the un baffled and baffled cases have different time scales, shown at top and bottom of the graph, and that the time scale for the un baffled flow is roughly ten times smaller than that for the baffled case.

This result indicates that the interior geometry of shafts and stairways can have a significant effect on the upward spreading rate of the hot gas plume. Although viscous effects may have an effect on these results, the baffles clearly have a very large effect and we should expect that the contents of stairwells will have a marked influence on the turbulent mixing process in real fire-scale configurations.

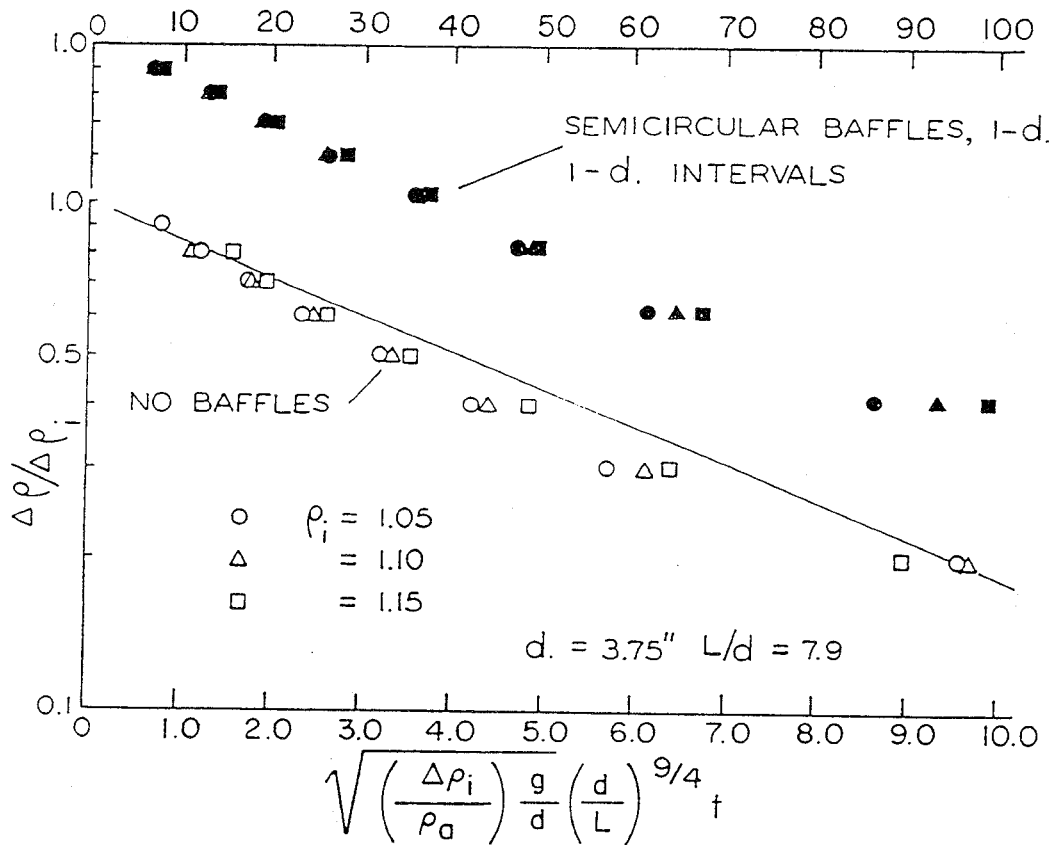


Figure 16. Influence of Baffles on Propagation of the Front

10. Conclusions

The turbulent mixing process examined here can transport hot gases vertically in buildings through shafts or other vertical openings with and without the stack effect. Models for the turbulent mixing process developed here are not entirely satisfactory but they give a reasonable picture of the experimental results and the limited success of these modeling efforts suggests that better models that include heat transfer can be developed.

The final forms for the diffusion coefficient and the mass flux across a horizontal surface within a shaft with area A_p are given by

$$\mathcal{D}_t = k \sqrt{\frac{1}{\rho_a} \left(\frac{\partial \rho}{\partial Z} \right) g} d^2 \left(\frac{L}{d} \right)^{\frac{1}{4}} \quad \text{and} \quad A_p \mathcal{D}_t \left(\frac{\partial \rho}{\partial Z} \right) \Big|_z$$

and the experimental data suggests that $k \approx 0.28$.

The analysis discussed above gives the general trends for the data and does lead to relatively simple and accurate models of the flow in several configurations of interest. The basic dimensional representations of the variables appears to be satisfactory and the model predicts the decay of the density difference within the shaft remarkably well given the simplifications used in the derivation of the solutions.

Data correlations based on the simple model are not completely consistent. For example, the dependence of the local turbulent diffusivity on the length of the tube and the variation from the predicted values (α / k) are problems. At least in part, these problems are thought to be caused by the simplification of the continuity equation as discussed above and a more rigorous treatment will be required to eliminate them. Thus, we believe that the primary problems with the current analysis are that the Boussinesq approximation is made in the diffusion term and that the convective transport due to density changes is neglected.

These approximations can be corrected although numerical rather than algebraic solutions will be required. A computation scheme that will correct these deficiencies in the model, and that will allow large density differences and heat transfer to the walls of the shaft is currently under development.

NIST-114 (REV. 6-93) ADMAN 4.09	U.S. DEPARTMENT OF COMMERCE NATIONAL INSTITUTE OF STANDARDS AND TECHNOLOGY	(ERB USE ONLY)						
MANUSCRIPT REVIEW AND APPROVAL		<table border="1" style="width:100%; border-collapse: collapse;"> <tr> <td style="width:50%;">ERB CONTROL NUMBER</td> <td style="width:50%;">DIVISION</td> </tr> <tr> <td style="width:50%;">PUBLICATION REPORT NUMBER NIST-GCR-95-679</td> <td style="width:50%;">CATEGORY CODE</td> </tr> <tr> <td style="width:50%;">PUBLICATION DATE October 1995</td> <td style="width:50%;">NUMBER PRINTED PAGES</td> </tr> </table>	ERB CONTROL NUMBER	DIVISION	PUBLICATION REPORT NUMBER NIST-GCR-95-679	CATEGORY CODE	PUBLICATION DATE October 1995	NUMBER PRINTED PAGES
ERB CONTROL NUMBER	DIVISION							
PUBLICATION REPORT NUMBER NIST-GCR-95-679	CATEGORY CODE							
PUBLICATION DATE October 1995	NUMBER PRINTED PAGES							

INSTRUCTIONS: ATTACH ORIGINAL OF THIS FORM TO ONE (1) COPY OF MANUSCRIPT AND SEND TO THE SECRETARY, APPROPRIATE EDITORIAL REVIEW BOARD

TITLE AND SUBTITLE (CITE IN FULL)

A REVIEW OF FLOWS DRIVEN BY NATURAL CONVECTION IN ADIABATIC SHAFTS

CONTRACT OR GRANT NUMBER Grant No. 60NANB6D1444	TYPE OF REPORT AND/OR PERIOD COVERED
--	--------------------------------------

AUTHOR(S) (LAST NAME, FIRST INITIAL, SECOND INITIAL) Zukoski, E.E. Department of Mechanical Engineering California Institute of Technology Pasadena, CA 91125	PERFORMING ORGANIZATION (CHECK (X) ONE BOX) <input type="checkbox"/> NIST/GAITHERSBURG <input type="checkbox"/> NIST/BOULDER <input type="checkbox"/> JILA/BOULDER
---	---

LABORATORY AND DIVISION NAMES (FIRST NIST AUTHOR ONLY)
 Building and Fire Research Laboratory/Fire Modeling and Applications Group

SPONSORING ORGANIZATION NAME AND COMPLETE ADDRESS (STREET, CITY, STATE, ZIP)
 U.S. Department of Commerce
 National Institute of Standards and Technology
 Gaithersburg, MD 20899

PROPOSED FOR NIST PUBLICATION

<input type="checkbox"/> JOURNAL OF RESEARCH (NIST JRES)	<input type="checkbox"/> MONOGRAPH (NIST MN)	<input type="checkbox"/> LETTER CIRCULAR
<input type="checkbox"/> J. PHYS. & CHEM. REF. DATA (JPCRD)	<input type="checkbox"/> NATL. STD. REF. DATA SERIES (NIST NSRDS)	<input type="checkbox"/> BUILDING SCIENCE SERIES
<input type="checkbox"/> HANDBOOK (NIST HB)	<input type="checkbox"/> FEDERAL INF. PROCESS. STDS. (NIST FIPS)	<input type="checkbox"/> PRODUCT STANDARDS
<input type="checkbox"/> SPECIAL PUBLICATION (NIST SP)	<input type="checkbox"/> LIST OF PUBLICATIONS (NIST LP)	<input type="checkbox"/> OTHER _____
<input type="checkbox"/> TECHNICAL NOTE (NIST TN)	<input type="checkbox"/> NIST INTERAGENCY/INTERNAL REPORT (NISTIR)	

PROPOSED FOR NON-NIST PUBLICATION (CITE FULLY) U.S. FOREIGN

PUBLISHING MEDIUM
 PAPER CD-ROM
 DISKETTE (SPECIFY) _____
 OTHER (SPECIFY) _____

SUPPLEMENTARY NOTES

ABSTRACT (A 2000-CHARACTER OR LESS FACTUAL SUMMARY OF MOST SIGNIFICANT INFORMATION. IF DOCUMENT INCLUDES A SIGNIFICANT BIBLIOGRAPHY OR LITERATURE SURVEY, CITE IT HERE. SPELL OUT ACRONYMS ON FIRST REFERENCE.) (CONTINUE ON SEPARATE PAGE, IF NECESSARY.)

Experimental and analytic studies of the motion of hot gases through vertical shafts under the influence of buoyancy forces, carried out from 1973 to 1976 at the California Institute of Technology, are reviewed. Such flows originate in and have a hazardous effect during accidental fires in facilities that involve vertical shafts.

Two mechanisms are primarily responsible for vertical motion of buoyant gas within a building: *stack effect* and the *turbulent mixing process*. This review focuses on the *turbulent mixing process*, where the vertical dimension of spaces of interest is much larger than the horizontal, i.e., relatively tall shafts. Particular emphasis of the work reviewed is on the transient development of the mixing process within the shaft as hot buoyant gas (e.g., smoke) is introduced into the lower part of a shaft, which is at some initial, uniform, and relatively low temperature.

KEY WORDS (MAXIMUM OF 9; 28 CHARACTERS AND SPACES EACH; SEPARATE WITH SEMICOLONS; ALPHABETIC ORDER; CAPITALIZE ONLY PROPER NAMES)
 buoyant flow; heat transfer; high rise buildings; high temperature gases; leakage; smoke; stack effect; turbulent mixing

AVAILABILITY

<input checked="" type="checkbox"/> UNLIMITED	<input type="checkbox"/> FOR OFFICIAL DISTRIBUTION - DO NOT RELEASE TO NTIS
ORDER FROM SUPERINTENDENT OF DOCUMENTS, U.S. GPO, WASHINGTON, DC 20402	
<input checked="" type="checkbox"/> ORDER FROM NTIS, SPRINGFIELD, VA 22161	

NOTE TO AUTHOR(S): IF YOU DO NOT WISH THIS MANUSCRIPT ANNOUNCED BEFORE PUBLICATION, PLEASE CHECK HERE.